105
21

CHARACTERIZATION OF MOLECULAR POTENTIAL ENERGY SURFACES:
CRITICAL POINTS, REACTION PATHS, AND REACTION VALLEYS

Elfi Kraka[1] and Thom H. Dunning, Jr.

Advances in Molecular Electronic Structure Theory,
Volume 1, pages 129-173.

ISBN: 0-89232-956-4

ABSTRACT

The discussion focuses on the systematic exploration and characterization of molecular potential energy surfaces. The emphasis is two-fold: (*i*) presentation of the theoretical methodology which has been developed to characterize complex multi-dimensional energy functions and (*ii*) extraction of simple, useful, yet theoretically sound chemical concepts from the formal mathematical analysis. First, location and characterization of *critical points* on potential surfaces are discussed: *minima* correspond to the equilibrium structures of reactants and products while *saddle points* correspond to transition structures connecting the reactants and products. Next, the *reaction path* connecting the critical points is discussed. The *intrinsic* reaction path (*IRC*) is the classical path that the molecular system would follow if the excess kinetic energy were continually dissipated; the *IRC* forms the basis for the *reaction path Hamiltonian* description of the dynamics of chemical reactions. Specification of the terms in the reaction path Hamiltonian requires information not only on the *IRC* but also on the *reaction valley* surrounding the *IRC*. These terms provide a direct connection between the features of the potential energy surface and the reaction dynamics. The use of reaction path concepts is illustrated for the OH + H_2 reaction, which is one of the few polyatomic reactions for which extensive experimental and theoretical studies have been reported. It is shown that even subtle features of the reaction dynamics can be understood with this approach.

1. INTRODUCTION

Theoretical understanding of the detailed mechanisms of chemical reactions is one of the ultimate goals in chemistry. Computation of the energetics and dynamics of chemical reactions requires a detailed knowledge of the interactions between the atomic and/or molecular species involved in the reaction. The dependence of these interactions on the positions of the nuclei defines the molecular potential energy surface. Thus the potential energy surface plays a central role in our understanding of chemical reactivity.

The potential energy surface $V(\mathbf{R})$ for a molecule composed of N atoms

is a function of ($3N$–6) internuclear coordinates (**R**), i.e., 6 variables for a four-atom system, 12 variables for a six-atom system, etc. Calculation and characterization of this multidimensional function present one of the major challenges in modern theoretical chemistry. During the past few years a number of potential energy surfaces for three-, four-, and more atom systems have been explored [1–7] (see also the chapter by L. B. Harding); this has been made possible by rapid advancement on both theoretical methodology and computer technology. Even given these advances, however, three major problems remain: (1) the calculation of reaction energies to chemical accuracy, i.e., better than 1 kcal/mol, remains an elusive goal for any save the simplest reactions, (2) a general procedure for obtaining accurate, analytic represention of potential energy surfaces has not yet been developed, and (3) the complex, multidimensional potential energy function is not in a form that can be readily analyzed, i.e., the important chemical information extracted and condensed into simple, useful, yet theoretically sound, chemical concepts. The first problem was discussed in the chapter by L. Harding, the second in the chapter by G. Schatz; in this chapter we will address the third problem.

In this chapter we will focus on the systematic exploration and characterization of molecular potential energy surfaces. We will start by locating and characterizing the *critical points* on the potential energy surface; these points play a dominant role in delimiting the overall reaction energetics and rates. Next we will determine the *reaction path* connecting these points; the reaction path provides information on the detailed motions of the nuclei during the reactive encounter. Finally we will explore the valley surrounding this path. Characterization of the *reaction valley* provides a direct connection between the dynamics of the chemical reaction and the features of the potential energy surface. The OH + H_2 reaction will be the test case for these new concepts, because it is one of the few reactions involving more than three atoms for which extensive experimental and theoretical studies have been reported.

2. CRITICAL POINTS ON MOLECULAR POTENTIAL ENERGY SURFACES

Although the molecular potential energy surface is a global function of the internal coordinates of the molecule, fortunately, not all regions of a surface are of equal importance. Regions of greatest importance include minima and saddle points of first order. Minima correspond to the equilibrium

structures of stable molecules: the *global* minimum corresponds to the energetically most stable conformation of the molecule and *local* minima to higher energy conformers. A *saddle point of first order* is the highest energy configuration on the minimum energy path connecting two minima [8]. It is the *mountain pass* separating the reactant valley from the product valley that must be surmounted before the chemical reaction can take place (ignoring tunneling, of course). Both minima and saddle points of first order are stationary or critical points. At these points all of the first derivatives of the energy $V(\mathbf{R})$, i.e., the gradient, vanish

$$g_k = \frac{\partial V}{\partial R_k} = 0 \tag{1}$$

Thus, at critical points there are no internal forces on the atoms.

Critical points can be characterized by the matrix of second derivatives of the energy, the Hessian or force constant matrix, with elements

$$H_{kl} = \frac{\partial^2 V}{\partial R_k \partial R_l} \tag{2}$$

At a minimum, the eigenvalues of the Hessian matrix, $\{\lambda_i\}$, are all positive (the Hessian is positive definite). That is, at these points the energy surface is everywhere concave upward (as it must be for a minimum!). For saddle points of first order there is one and only one negative eigenvalue of the Hessian matrix. In this case, the surface is a minimum in $(3N-7)$ dimensions; in the other dimension, it is a maximum. Since the molecular potential energy surface is a smooth function connecting the minima, i.e., it is contiguous, there must be at least one saddle point of first order between two connected minima. There are in fact, at least $(m-1)$ saddle points of first order on a surface with m minima [9].

Besides minima and saddle points of first order a molecular potential energy surface may possess maxima (all eigenvalues negative) or saddle points of higher order n (n negative eigenvalues and $3N-6-n$ positive eigenvalues with $n>1$). However, it is always possible to find a lower energy path around these points, and consequently they are usually not important in the description of chemical reactions. Higher order saddle points will not be considered in this chapter. In the following we will use the term saddle point synonymously for saddle point of first order.

2.1 Location of Critical Points

Over the past few years a number of methods have been developed to locate critical points (minima and/or saddle points) on molecular potential energy surfaces [10,11]. A detailed discussion of these techniques would be beyond the scope of this chapter. In addition, it is difficult to assess the usefulness of any specific algorithm quantitatively, since the results strongly depend on the particular application at hand. Thus, we restrict ourselves to a brief discussion highlighting the general aspects of these techniques.

Methods for locating minima and/or saddle points can be grouped into three categories depending on the information required [12–15]. The most accurate and stable methods are Newton methods, which use the energy and the first (gradient) and second (Hessian) derivatives. Methods have also been developed that are based on the energy and gradient and on the energy only. Energy-only methods have the widest range of applicability since they do not require any derivatives. However, they often exhibit slow convergence. Since gradients and Hessians can be computed analytically for an ever increasing variety of wavefunctions [16,17], methods that rely solely on the energy are being used less and less frequently.

One well-known representative of the Newton methods is the Newton–Raphson method [18] where the function, in our case the potential energy surface $V(\mathbf{R})$, is approximated at a point $\mathbf{R}_0$ close to the critical point $\mathbf{R}_c$ by a Taylor series expansion about $\mathbf{R}_0$

$$V(\mathbf{R}) = V_0(\mathbf{R}) + \sum_{k=1}^{3N-6} g_k(\mathbf{R}_0)\Delta R_k + \frac{1}{2}\sum_{k=1}^{3N-6}\sum_{l=1}^{3N-6} H_{kl}(\mathbf{R}_0)\Delta R_k \Delta R_l \tag{3}$$

with the expansion truncated at the second order (Hessian) terms. In (3) ΔR_k is defined as

$$\Delta R_k = R_k - R_{0k}$$

In matrix-vector notation (3) can be written

$$V(\mathbf{R}) = V_0(\mathbf{R}_0) + \mathbf{g}^{\mathrm{T}}\,\Delta\mathbf{R} + \tfrac{1}{2}\Delta\mathbf{R}^{\mathrm{T}}\,\mathbf{H}\Delta\mathbf{R} \tag{4}$$

At a critical point the condition (1) must be satisfied which leads to

$$\Delta \mathbf{R} = -\mathbf{H}^{-1}\mathbf{g} = -\mathbf{A}\mathbf{g} \tag{5}$$

where $\mathbf{A}$ is the inverse of the Hessian.

Equation (5) defines the Newton–Raphson (NR) step. This is the step to take in order to get from the current point to the stationary point, provided, of course, that $V(\mathbf{R})$ is truly quadratic over the region $\mathbf{R}_0 \rightarrow \mathbf{R}_c$. Since this is usually not the case, an iterative procedure is required. To determine if the new point, $\mathbf{R}_{new} = \mathbf{R}_0 + \Delta\mathbf{R}$, predicted by (5), is indeed a stationary point, $\mathbf{g}(\mathbf{R}_{new})$ is computed. If $|\mathbf{g}(\mathbf{R}_{new})|$ is above a preset threshold, say ε where ε is small, the above procedure is repeated until $|\mathbf{g}(\mathbf{R}_{new})| \leq \varepsilon$.

Because of the nonquadratic nature of molecular potential energy surfaces, the vector $\Delta\mathbf{R}$ obtained in the NR step usually under- or overshoots the true critical point. To correct this problem, the length of the correction vector can be adjusted by determining the point along $\Delta\mathbf{R}$ for which the energy or $|\mathbf{g}|$ is a minimum [19], i.e., α is adjusted to minimize $E(\mathbf{R}_0 + \alpha\Delta\mathbf{R})$ or $|\mathbf{g}(R_0 + \alpha\Delta\mathbf{R})|$. This procedure ensures that the new point is the optimum point along the correction vector for the next iteration. It does, however, require additional evaluations of the energy and/or gradient.

Since analytic first and second derivatives are available for a variety of wavefunctions, Newton-type methods would appear to be the methods of choice. However, a caveat is appropriate. At present the cost of computing second derivatives is substantially more than the cost of computing the energy and gradient. Therefore, in most cases the Hessian is not computed directly during the iterative search for the critical point. If the Hessian is simply taken to be the unit matrix (or a constant times a unit matrix), the search is along

$$\Delta\mathbf{R} = -\mathbf{g} \tag{6}$$

As we shall see later, the function decreases most rapidly along the negative of the gradient. The step (6) thus defines the steepest descent method [20], the simplest representative of gradient methods. More elaborate gradient methods approximate the Hessian matrix; they are usually referred to as quasi-Newton methods[21]. An initial Hessian matrix (which may be the unit matrix) is updated at each iteration in the search, based on the computed changes in the gradient. Quasi-Newton methods differ by the initial guess for the Hessian [22] and the manner in which the Hessian or its inverse is updated [23].

One of the most often used quasi-Newton methods is the Davidson–

Fletcher–Powell (DFP) algorithm [24]. Since the steepest descent method shows best convergence at points far away from the stationary point while the Newton–Raphson method works best near this point [25], the DFP method was designed to yield a stepwise transition from a pure steepest descent step toward a Newton-type step during the course of the search. Hence, the first step is in the direction of the steepest descent, i.e., the initial Hessian matrix is the unit matrix. In subsequent iterations the inverse Hessian matrix is updated by the following scheme:

$$\mathbf{A}^m = \mathbf{A}^{m-1} + \frac{\Delta\mathbf{R}^m(\Delta\mathbf{R}^m)^\mathsf{T}}{(\Delta\mathbf{R}^m)^\mathsf{T}\Delta\mathbf{g}^m} - \frac{\mathbf{A}^{m-1}\Delta\mathbf{g}^m(\Delta\mathbf{g}^m)^\mathsf{T}\mathbf{A}^{m-1}}{(\Delta\mathbf{R}^m)^\mathsf{T}\,\mathbf{A}^{m-1}\Delta\mathbf{g}^m} \tag{7}$$

where m denotes the iteration number and

$$\Delta\mathbf{R}^m = \boldsymbol{R}^m - \mathbf{R}^{m-1}$$

$$\Delta\mathbf{g}^m = \mathbf{g}^m - \mathbf{g}^{m-1}$$

Another updating scheme for the inverse Hessian was proposed by Murtagh and Sargent [26]. They also start with a steepest descent step, but $\mathbf{A}$ is updated according to

$$\mathbf{A}^m = \frac{[\Delta\mathbf{R}^m - \mathbf{A}^{m-1}\Delta\mathbf{g}^m]\,[\Delta\mathbf{R}^m - \mathbf{A}^{m-1}\Delta\mathbf{g}^m]^\mathsf{T}}{[\Delta\mathbf{R}^m - \mathbf{A}^{m-1}\Delta\mathbf{g}^m]^\mathsf{T}\Delta\mathbf{g}^m} \tag{8}$$

Whereas quasi-Newton methods evaluate the approximate Hessian or its inverse explicitly, conjugate gradient algorithms [27] avoid the direct evaluation of these matrices. As such they are not quasi-Newton methods in a strict sense. Conjugate gradient methods are suitable for large molecules, where the storage of the Hessian matrix is not practicable. A typical representative of these methods is the Fletcher–Reeves approach [28]. Here the correction vector $\Delta\mathbf{R}$ for the mth iteration step is given by

$$\Delta\mathbf{R}^m = -\mathbf{g}^m\,\Delta\mathbf{R}^{m-1}\left[\frac{(\mathbf{g}^m)^\mathsf{T}\,\mathbf{g}^m}{(\mathbf{g}^{m-1})^\mathsf{T}\,\mathbf{g}^{m-1}}\right] \tag{9}$$

Most quasi-Newton and conjugate gradient methods use only the change in the gradient from the previous step in their updating schemes. A new

algorithm advanced by Schlegel [29] considers the gradient changes of all (m–1) previous steps. This promises improved convergence properties.

While the above techniques have revolutionized the calculation of equilibrium molecular structures, location of saddle points poses special problems. Unlike a minimum, a first-order saddle point must be a maximum in one (and only one!) direction. And this direction is not known in advance (except in unusual cases) and must be found during the search process. Most of the quasi-Newton methods, like the ones described so far (with the exception of Schlegel's method), can be used only for locating minima because they require a positive-definite Hessian matrix. Location of a saddle point can, of course, be changed into a minimization. Since $\mathbf{g}$ is zero for each critical point, saddle points as well as minima may be located by minimizing the gradient norm. Probably the most common method used in saddle point calculations is minimization of the square of the gradient norm, $|\mathbf{g}|^2$, by standard least-squares minimization techniques. This approach was originally proposed by McIver and Komornicki [30].

If both first and second derivatives of the energy are available, Newton methods can be used to locate saddle points. These methods require that the Hessian at the initial point have one and only one negative eigenvalue for the search to converge. For example, at any point on the surface the NR step (5) can be rewritten in terms of the eigenvectors and eigenvalues, $\{\mathbf{v}_k\}$ and $\{\lambda_k\}$, of the local Hessian matrix as [31]

$$\Delta\mathbf{R} = \sum_{k=1}^{3N-6} \frac{-\mathbf{v}_k^{\top}\,\mathbf{g}\mathbf{v}_k}{\lambda_k} \tag{10}$$

In this representation it is clear that the NR step is directed opposite to the gradient for eigenmodes that have positive eigenvalues and along the gradient for eigenmodes that have negative eigenvalues. That is, if we are in a region for which the Hessian matrix has one negative eigenvalue and (n–1) positive eigenvalues, then the NR step minimizes the energy along the (n–1) bound (positive eigenvalue) modes and maximizes the energy along the unbound (negative eigenvalue) mode. This is, of course, just what is desired.

Unfortunately, it is often not possible to obtain initial estimates for saddle point geometries that satisfy the above condition—while the structures of stable molecules are reasonably well understood, the same cannot be said for saddle points. If the local Hessian matrix does not have the correct

structure, the NR step is no longer appropriate and a step must be chosen in a direction leading to the appropriate region. To address this problem, a quasi-Newton-like algorithm has been proposed by Simons and co-workers [31] and improved by Baker [32]. This algorithm, which incorporates the Hessian mode-following ideas of Cerjan and Miller [33], can locate transition states even if the Hessian matrix at the starting geometry has the wrong structure. In order to leave the region with the wrong Hessian structure, Cerjan and Miller [33] and Simon and co-workers [31] suggested a modified NR step in which a shift parameter, λ^s, is used to force the step in an appropriate direction

$$\Delta \mathbf{R} = \sum_{k=1}^{3N-6} \frac{-\mathbf{v}_k^T \mathbf{g} \mathbf{v}_k}{\lambda_k - \lambda^s} \tag{11}$$

Consider the case when all of the eigenvalues of the Hessian matrix are positive. If λ^s is chosen such that $(\lambda_k - \lambda^s)$ is negative for the first eigenvalue and positive for all of the remaining eigenvalues, the modified NR step will follow the least bound mode uphill toward a saddle point while simultaneously minimizing the energy along the other $(n-1)$ modes. Simons and co-workers [31b] used a rational function optimization to determine the shift parameter, a procedure that is equivalent to scaling all of the coordinates. In fact, for a transition state search they showed that two shift parameters, $\lambda^{s,p}$ and $\lambda^{s,n}$, could be used: one for the first mode relative to which the energy is to be maximized and one for the other $(n-1)$ modes for which it is minimized. These parameters were determined from a set of eigenvalue equations (see, however, Baker [32]).

In a transition state search starting from a minimum (or a region in which all of the eigenvalues of the Hessian are positive), it is assumed that maximization takes place along the lowest energy hessian mode, λ_1, and minimization along all higher modes. This has been generalized in Baker's algorithm [32], i.e., one can maximize along modes other than the lowest and in this way transition states for alternative rearrangements and/or dissociations from the same initial starting point can be located.

2.2 Characterization of Critical Points

The equilibrium geometries, fundamental frequencies, and other molecular properties of the reactants and products, corresponding to minima

on the molecular potential energy surface, may be obtained experimentally by the use of a variety of spectroscopic methods [34]. However, the properties of transition structures, corresponding to saddle points on the potential energy surface, cannot be obtained from experiment, at least not at present [35]. Although qualitative information about transition states may be inferred from kinetic isotope effects [36] and activation entropies [37], the only way to characterize saddle points in detail is by calculation!

Saddle points on the potential energy surface play a central role in governing the reaction mechanism. The height of the *barrier to reaction* is just the difference in energy between the reactant minimum and the saddle point:

$$\Delta E_{\text{barrier}} = V(\mathbf{R}^{\text{sp}}) - V(\mathbf{R}^{\text{r}}) \tag{12}$$

The *reaction energy defect* is

$$\Delta E_{\text{rxn}} = V(\mathbf{R}^{\text{p}}) - V(\mathbf{R}^{\text{r}}) \tag{13}$$

In (12) and (13) $\mathbf{R}^{\text{p}}$ refers to the product equilibrium geometry, $\mathbf{R}^{\text{r}}$ to the reactant geometry, and $\mathbf{R}^{\text{sp}}$ to the saddle point geometry. Since V is negative, the products are lower in energy than reactants if ΔE_{rxn} is negative.

To calculate the energetics of chemical reactions, we need, in addition to the structures and potential energies of the minima and saddle points, the frequencies of the bound vibrational modes at each of these points. The simplest procedure for determining the vibrational frequencies and associated normal modes constructs the Hessian matrix in mass-weighted cartesian coordinates [38]. The Hessian matrix in the $3N$ cartesian coordinates can be obtained from the Hessian matrix in the $(3N-6)$ internal coordinates by numerical differentiation, i.e., if the expansion of the energy in internal coordinates is given by

$$V(\mathbf{R}) = V_0(\mathbf{R}_0) + \tfrac{1}{2}\sum_{i=1}^{3N-6}\sum_{j=1}^{3N-6} H_{ij}(\mathbf{R}_0)\Delta R_i \Delta R_j \tag{14}$$

the Hessian matrix elements for the expansion in cartesian coordinates, $H_{ij}'(\mathbf{X}_0)$, can be obtained from (14) by numerically evaluating the second derivatives, i.e., calculating $\Delta^2 E(\mathbf{R})/\Delta X_i \Delta X_j$.

To compute the vibrational frequencies and normal modes, the Hessian

matrix in cartesian coordinates is transformed to mass-weighted cartesian coordinates where

$$x_i = \sqrt{M_i X_i} \tag{15}$$

This just involves dividing H_{ij}' by $\sqrt{M_{iA}M_{jB}}$ where A and B refer to the two nuclei corresponding to coordinates X_i and X_j. The eigenvalues of the mass-weighted Hessian matrix are the squares of the vibrational frequencies (ω_i^2); the eigenvectors (L_k) give the normal modes

$$Q_k = \sum_{i=1}^{3N} L_{ki}(x_i - x_{i0}) \tag{16}$$

where $\{x_0\}$ is the mass-weighted Cartesian coordinate of the critical point.

For a nonlinear polyatomic molecule diagonalization of the mass-weighted Cartesian Hessian matrix will yield six zero frequencies (five for linear polyatomics). These correspond to translation and rotation of the molecule as a whole. At a minimum all of the remaining (3*N*–6) nonzero eigenvalues will be positive and all of the frequencies real. At a saddle point there will be one negative eigenvalue of the Hessian matrix and, thus, one imaginary frequency—the *reaction frequency* (ω_{rxn}) *at the saddle point.* The normal mode associated with the imaginary frequency is the *reaction coordinate* ($\mathbf{Q}_{rxn}$) *at the saddle point.*

In the harmonic approximation the zero point energy for a stable molecule is simply

$$E_{zpe} = \frac{1}{2} \sum_{k}^{3N-6(7)} \hbar\omega_k \tag{17}$$

where the sum runs over (3*N*–6) frequencies. For saddle points the sum in (17) runs over only the (3*N*–7) real frequencies. Using this definition and the earlier definitions given for the reaction energy defect and the classical barrier height, we can now compute the energetics of chemical reactions including vibrational effects. The *enthalpy change at 0 K* and the *vibrationally adiabatic threshold* for a chemical reaction are given by

$$\Delta H_0 = \Delta E_{rxn} + (E_{zpe}^{p} - E_{zpe}^{r}) \tag{18}$$

$$\Delta E_{vat} = \Delta E_{barrier} + (E^{sp}_{zpe} - E^{r}_{zpe}) \tag{19}$$

where E^{i}_{zpe} is the zero point energy for conformation i.

The above takes into account only the quadratic (or harmonic) terms in the potential energy expansion. If higher order terms are included, the vibrational energy levels are given by [39]

$$G(v_1, v_2, \ldots) = \sum_{k=1}^{3N-6} \hbar\,\omega_k(v_k + \frac{1}{2}) + \sum_{k=1}^{3N-6}\sum_{l=1}^{3N-6} A_{kl}\,(v_k + \frac{1}{2})(v_l + \frac{1}{2}) \tag{20}$$

where v_k denotes the vibrational eigenstate of mode k and A_{kl} is the anharmonicity constant coupling mode k and l. A detailed discussion of the calculation of vibrational and rotational constants of polyatomic molecules is given in the chapter by W. C. Ermler and H. C. Hsieh.

While the critical points on the potential energy surface provide valuable information about the reaction energy and the barrier to reaction, i.e., whether a reaction is energetically favorable, little can be said about the detailed mechanism of the reaction. Thus we next explore the potential energy along a path connecting reactants, transition state, and products—this is the reaction path.

3. REACTION PATHS ON MOLECULAR POTENTIAL ENERGY SURFACES

Although the critical points on a potential energy surface are clearly defined in a mathematical and chemical sense, this is no longer true for the reaction path even though this concept is intimately connected with the mechanism of a chemical reaction [40–43]. To compound the confusion, the term reaction path is often used interchangeably with terms such as "reaction coordinate," "steepest descent path," "path of least energy," and "minimum energy path." Hence, first of all, it is of paramount importance to determine which of the available reaction paths is best suited for characterizing molecular potential energy surfaces. Our guidelines will be the basic requirements every useful chemical model should fulfill: It should be simple and easy to understand; it should possess a sound physical basis; it should provide a consistent description of its objects; and it should be flexible and applicable over as wide a range as possible.

3.1 The "Distinguished" Reaction Coordinate

One way of defining a reaction path is based on the assumption that one of the internal coordinates varies monotonically during the course of the reaction. This particular coordinate is then defined as the *distinguished reaction coordinate*, R^{drc}. Stepping along this coordinate in the direction leading from reactants to products, i.e., for various values of R^{drc} the remaining internal coordinates, (R_k, k=1, $3N$–7), are optimized. The resulting coordinate set, $\mathbf{R}^{drp} = [R^{drc}, \{R_k^{opt}\}]$, defines the *distinguished reaction path*. The barrier to reaction is the highest energy point along the energy profile $V(\mathbf{R}^{drp})$.

Although simple to implement and to use, the above approach suffers from three major shortcomings. First, it is not always possible to identify an appropriate reaction coordinate with one of the internal coordinates. A simple example is the abstraction reaction

$$AB + C \rightarrow A + BC$$

for which one coordinate, R_{BC}, best describes the path in the entrance channel, while another, R_{AB}, should be used in the exit channel. Other examples include the pericyclic reactions [44], like Cope and Claisen rearrangements, electrocyclic and cycloaddition reactions, where several bonds are to be broken and formed in a synchronous process. Second, the above procedure does not guarantee that the reaction path so determined will pass over the lowest energy barrier separating reactants from products. Only in favorable cases [45] does the generated path approach the true transition point. Third, the other internal coordinates may depend discontinuously (or nearly discontinuously) on R^{drc} [46]. Such discontinuities are not the result of a mysterious reaction mechanism but simply reflect the strong coupling between the internal coordinates and the *arbitrarily* chosen reaction coordinate. A recent discission of the use and abuse of the "distinguished" reaction coordinate approach [47] makes it quite clear that this reaction path model is not appropriate for the present purpose.

3.2 The Steepest Descent Path

A more objective way to define the reaction path is to start at the saddle point separating reactants from products and follow the steepest descent path, in one direction to reactants and in the other direction to products.

Along the steepest descent path we always take a step that leads to the maximal decrease in the energy. As we noted earlier, the steepest descent path follows the gradient of the potential energy surface. To see this, let us expand the energy about a point, $\mathbf{R}_0$, on the steepest descent path retaining only the linear terms:

$$\Delta V(\mathbf{R}) = V(\mathbf{R}) - V(\mathbf{R}_0) = \sum_k \frac{\partial V}{\partial R_k} \Delta R_k = \sum_k g_k \Delta R_k \tag{21}$$

We now wish to take a step of fixed length

$$\Delta \mathbf{R}^2 = \sum_k \Delta R_k^2 \tag{22}$$

such that the energy decreases by the maximum amount possible. To do this, we must minimize the energy functional:

$$I(\mathbf{R}) = \sum_k g_k \Delta R_k + \frac{1}{2\alpha} \sum_k \Delta R_k^2 \tag{23}$$

where $(1/2\alpha)$ is the Lagrange multiplier associated with the constraint (22). This yields

$$\Delta R_k = -\alpha g_k \tag{24}$$

Thus, along the steepest descent path the length of the step in any given internal coordinate is proportional to the negative of the gradient of the energy in that direction. It has been shown that the steepest descent path passes continuously from reactants to products through the saddle point [48].

Note that in differential form the set of equations (24) can be rewritten as

$$\frac{dR_1}{g_1} = \frac{dR_2}{g_2} = \frac{dR_3}{g_3} = \cdots \tag{25}$$

The significance of this form of the steepest descent equations will become apparent later.

At the saddle point the gradient, of course, vanishes. Thus, the above procedure does not define the direction of the path right at the saddle point. To do so, we must expand the energy to second order and minimize the resulting functional. This yields the matrix equation

$$(\mathbf{H} - \lambda \mathbf{I})\,\Delta\mathbf{R} = \mathbf{0} \tag{26}$$

where $\mathbf{I}$ is the unit matrix. At a saddle point this matrix has one negative eigenvalue. The reaction coordinate at the saddle point leads down off the saddle into the reactant and product wells. Stepping along this coordinate results in the maximum decrease in the molecular energy. Thus, at the saddle point the steepest descent path follows the reaction coordinate.

Although the above provides a continuous path leading from reactants through the saddle point to products, it should be noted that it is still little more than a mathematical recipe, albeit a very reasonable one. It is not clear that the steepest descent path is connected in any way to the dynamics of the reaction. In addition, it depends on the choice of the coordinate system. This latter point has generated much debate [49–51]. The above choice of reaction path was first suggested by Fukui [52], although the concept appears to have a long history.

Instead of following the gradient one could also follow gradient extremals. These are curves that are locally defined by the requirement that the gradient is an eigenvector of the Hessian at each point on the curve [53]. Again, such curves are not necessarily related to the reaction dynamics in any simple way.

3.3 The Intrinsic Reaction Coordinate

Although the steepest descent path as outlined above is not clearly connected with the dynamics of the reaction, the intrinsic reaction coordinate[2] (*IRC*), which is simply the steepest descent path in mass-weighted cartesian coordinates, is. The first use of this path to describe reaction dynamics appears to have been by Shavitt [54] although it was mentioned by Eliason and Hirschfelder [55] at approximately the same time. Use of the intrinsic reaction coordinate to describe reaction dynamics has been investigated in great detail by Fukui and co-workers [56]. The *IRC* is computed as described above; the only difference is that instead of $3N$–6 internal coordinates $\mathbf{R}$ we use mass-weighted cartesian coordinates, defined in (15).

The intimate connection between the *IRC* and the reaction dynamics becomes obvious if the classical equations of motion for the nuclei moving on the potential energy surface are considered. The classical equations of motion are simply [57]

$$\frac{d}{dt}(M_i\dot{X}_i) = -\frac{\partial V}{\partial X_i} = -g_i \tag{27}$$

If, starting from the saddle point, the nuclei move with an infinitesimal velocity toward either reactants or products, (27) can be integrated to yield

$$M_i\dot{X}_i = -g_i t \tag{28}$$

or in mass-weighted coordinates

$$\frac{dx_i}{g_i} = -t\,dt \tag{29}$$

Thus, at any given time,

$$\frac{dx_1}{g_1} = \frac{dx_2}{g_2} = \frac{dx_3}{g_3} = \ldots \tag{30}$$

which is simply a restatement of the steepest descent equations, (25), in mass-weighted Cartesian coordinates. In other words, the *IRC* corresponds to the classical trajectory obtained by starting at the saddle point and moving with a constantly damped velocity toward either the reactants or the products (*trajectory-in-molasses*). In addition, since the classical equations of motion are independent of the choice of the coordinate system, the *IRC* is uniquely defined.

Although the use of $3N$ Cartesian coordinates to calculate the *IRC* is straightforward, Cartesian coordinates are not suitable for representing the potential energy surface, since the potential energy is only a function of the $(3N–6)$ internal coordinates. It does not depend on translational or rotational motions, which are included in the Cartesian coordinates. Thus, to describe the motion of the nuclei on a potential energy surface we need to back transform from the $3N$ mass-weighted cartesian coordinates ($\mathbf{x}$) to the set of $(3N–6)$ internal coordinates ($\mathbf{R}$), where the three translations and three rotations are eliminated by the center of mass and Eckart conditions [58].

However, the space in which the internal motions are separated from translations and rotations is not Euclidean. Unlike the space spanned by the $3N$ Cartesian coordinates, the space spanned by the internal coordinates is Riemanian [59]. With the definition of an appropriate metric in this space, given by the tensor elements $a_{k,l}$

$$a_{k,l} = \sum_i \left(\frac{\partial x_i}{\partial R_k}\right)\left(\frac{\partial x_i}{\partial R_1}\right) \tag{31}$$

the *IRC* equation in terms of internal (or generalized) coordinates (**R**) reads:

$$\sum_k a_{1,k}\left(\frac{dR_1}{g_1}\right) = \sum_k a_{2,k}\left(\frac{dR_2}{g_2}\right) = \sum_k a_{3,k}\left(\frac{dR_3}{g_3}\right) = \cdots \tag{32}$$

It should be stressed that for all sets of generalized coordinates (**R**), derived from the $3N$ mass-weighted cartesian coordinates by the use of Eq. (31), solution of (32) will yield the same *IRC* path. Hence, the problem of the coordinate dependence of the steepest descent path is solved in a very elegant way.

Fukui and co-workers [60] used the techniques of differential geometry to explore the properties of the *IRC*. In particular, they derived a variational principle for chemical reactions and showed that the *IRC* was the shortest path from a minimum to the saddle point with the length being equal to the barrier height [60b,d]. Igawa and Fukutone [61] showed that the *IRC* corresponds to the least motion path, i.e., it is the most favorable reaction path according to the principle of least motion in chemical reactions [62]. In addition to the discussion of the *IRC* within the framework of variation principles, a statistical interpretation of the *IRC* has been proposed [63].

Thus the *IRC* certainly appears to be an appropriate model for describing chemical reactions. It is uniquely defined, mathematically rigorous, and conceptually appealing; in addition, it is expected to be intimately related to the reaction dynamics. Once the *IRC* has been determined, the evolution of the molecular system along the *IRC* can be displayed. For example, plots of the internal coordinates along the *IRC* provide valuable information about the way the reacting atoms approach each other, interact, and then separate. In the case of polyatomic systems these two-dimensional pictures display the complex structural changes taking place in $3N$–6 dimensional space in a very understandable form [64] and can be used to generate three-dimen-

sional images of the structural changes along the reaction path. Plots of the molecular orbitals (in localized form) or the molecular electron density along the *IRC* provides valuable insight into electronic effects which govern the reaction [65,66]. GVB orbitals [67] are especially suited for this purpose since they provide a lucid and cogent orbital description of the electronic structure changes during the course of the reaction. Possible pathways may then be discussed within the framework of the "Orbital Phase Continuity Principle" [68] which is the valence-bond analog of the Woodward–Hoffmann Rules.

3.4 Calculation of the Intrinsic Reaction Path

Although the definition of the *IRC* is simple and straightforward, calculating the *IRC* presents a mathematical challenge. For any point $\mathbf{x}_s(s_0)$ on the reaction path, except at the saddle point, the reaction path can be represented as a Taylor series in s expanded about $\mathbf{x}_s(s_0)$:

$$\mathbf{x}_s(s) = \mathbf{x}_s(s_0) + \mathbf{c}_s^{(1)}(s-s_0) + \frac{1}{2}\mathbf{c}_s^{(2)}(s-s_0)^2 + \ldots + \frac{1}{n!}\mathbf{c}_s^{(n)}(s-s_0)^n \tag{33}$$

where the expansion coefficients $\mathbf{c}_s^{(i)}$ depend only on the energy derivatives evaluated at $\mathbf{x}_s(s_0)$. In (33) the reaction path, $\mathbf{x}_s(s_0)$ depends parametrically on the path length s, which is defined as the mass-weighted cartesian distance along the path

$$ds^2 = \sum_i dx_i^2 \tag{34}$$

The first coefficients in the expansion are $\mathbf{c}_s^{(1)}(s)$, the normalized path tangent:

$$\mathbf{c}_s^{(1)}(s) = \frac{d\mathbf{x}_s(s)}{ds} = \frac{-\mathbf{g}}{|\mathbf{g}|} \tag{35}$$

and the curvature $\mathbf{c}_s^{(2)}(s)$, of the path:

$$\mathbf{c}_s^{(2)}(s) = \frac{d\mathbf{c}_s^{(1)}(s)}{ds} = \frac{d^2\mathbf{x}_s(s)}{ds^2} \tag{36}$$

which is obtained by differentiating (35) with respect to s by use of the chain rule ($\mathbf{g}$ depends on s only implicitly through its dependence on $\mathbf{x}$):

$$\mathbf{c}_s^{(2)}(s) = \frac{\mathbf{H}^x \mathbf{c}_s^{(1)}(s) - [\mathbf{c}_s^{(1)}(s)^\top \mathbf{H}^x \mathbf{c}_s^{(1)}(s)]}{|\mathbf{g}|} \tag{37}$$

where $\mathbf{H}^x$ is the Hessian matrix in mass-weighted cartesian coordinates. Higher derivatives $\mathbf{c}_s^{(n)}(s)$ can be obtained in a similar way; a general formula has been derived by Page and McIver [69]. The stability and effectiveness of the algorithms for calculating reaction paths strongly depend on the number of terms included in (33), which, in turn, depend on the availability of energy derivatives.

The most simple and hence commonly used methods are Euler methods, which use only the first two terms in (33), i.e., they require only the gradient. They trace out the reaction path by taking a series of small steps m in the steepest descent direction yielding the following iteration scheme:

$$\mathbf{x}_s(s_m + \delta s) = \mathbf{x}_s(s_m) - \delta s \frac{\mathbf{g}(s)}{|\mathbf{g}(s)|} \tag{38}$$

where δs is the stepsize. Unfortunately, gradient-following methods tend to be unstable. Unless very small stepsizes are taken ($\delta s \leq 0.001 \sqrt{u\, a_0}$ [70]), the resulting oscillations about the true *IRC* are unacceptably large. Molecular properties, such as bond lengths or bond angles and especially derivatives of the energy or bond lengths and angles, evaluated along the calculated path clearly reveal these oscillations [71].

In order to overcome this problem Ishida et al. [72] added a one-dimensional search step along the bisector of the old and new gradient to damp out these oscillations. Schmidt et al. [73] further refined this procedure. Instead of an explicit search along the bisector they compute only one additional point on the bisector and used a parabolic fit to interpolate to the minimum. It was found that step sizes of $\delta s = 0.1 \sqrt{u\, a_0}$ were usable and that less than 200 energy and gradient calculations could be used to map out the *IRC* for small molecules [72,73]. Müller and Brown [74] proposed a method, where a step of fixed length is taken and the direction is chosen to minimize the energy with respect to the $(n-1)$ remaining degrees of freedom. Although each step requires an $(n-1)$ dimensional optimization, large step sizes can be employed. An average of 10 steps is needed for walking from the saddle point to one of the minima. However, this approach

is not suitable for strongly curved paths. A refinement of Gonzales and Schlegel [75] addresses this deficiency. Here the new point is chosen so that the reaction path between the new and old points is an arc of a circle and the old and new gradients are tangent to this path. Thus this technique explicitly accounts for the curvature of the reaction path.

More sophisticated numerical techniques can also be used for solving (38). Our experience indicates that an integration solver [76] based on a predictor–corrector algorithm [77] that takes care of the stiffness problem [78] is very efficient. Using this technique, step sizes can be increased by more than a factor of 10 over the simple Euler method while maintaining high accuracy in all computed quantities [79].

If analytical gradients are not available, solution of (38) with numerical gradients is intractable even for tetraatomic systems if the points are calculated by a high quality *ab initio* method. In this case it is best to work with an analytic representation of the potential energy surface in the vicinity of the reaction path. In our work [80] this is done by defining the potential energy in terms of local force fields, evaluated from grids of energy points centered along an approximate reaction path, connected by switching functions. Using this technique it is possible to calculate the gradient numerically at sufficiently small step sizes to accurately and economically determine the reaction path. However a caveat is appropriate here. First, the reaction path is not known a priori; hence, the right choice of the grids is a matter of trial and error. Second, the use of switching functions leads to small, but significant, fluctuations in the derivatives of the energy and coordinates at the grid boundaries (see also the closing paragraph below). Third, depending on the quality of the fit, the reaction path obtained from the global representation may deviate from the true path.

If analytical second derivatives are also available a new reaction path following method recently proposed by Page and McIver [69] appears to be very promising. Fundamental to this new approach is a Taylor series expansion of the potential energy in terms of cartesian displacements. Expanding the energy to second order, i.e., a local quadratic approximation (LQA), and parameterizing the reaction path as suggested by Pechukas [81], they were able to sum (33) exactly. This procedure yields a reaction path that has the correct curvature at the point of expansion.

Pechukas [81] showed that if the reaction path is represented by a curve $\mathbf{x}(t)$ instead by a curve $\mathbf{x}_s(s)$ with

$$\frac{d\mathbf{x}(t)}{dt} = -\mathbf{g} \tag{39}$$

then (39) can be solved exactly when the energy is a quadratic function of the coordinates. Following this, Page and McIver derived the following equation for the gradient within the LQA:

$$g(\mathbf{x}) = \mathbf{g}_0 + \mathbf{H}_0(\mathbf{x}-\mathbf{x}_0) \tag{40}$$

where $\mathbf{g}_0$ and $\mathbf{H}_0$ are the gradient and Hessian evaluated at a point $\mathbf{x}_0 = \mathbf{x}(t=0)$ lying on the path (it cannot be the saddle point). Then the *IRC* is obtained by integrating

$$\frac{d\mathbf{x}}{dt} = -\mathbf{g}_0 - \mathbf{H}_0(\mathbf{x}-\mathbf{x}_0) \tag{41}$$

For computation convenience (41) is transformed to generalized normal coordinates and solved using iterative techniques [69].

For the first step from the saddle point, $\mathbf{x}^{sp}$, Page and McIver used a local cubic approximation (LCA) yielding the following equation:

$$\mathbf{x}_s(\mathbf{x}^{sp} + \delta s) = \mathbf{x}_0 + \mathbf{Q}_{rxn}\delta s + \tfrac{1}{2}\,\mathbf{K}(\delta s)^2 \tag{42}$$

where $\mathbf{Q}_{rxn}$ is the reaction coordinate and $\mathbf{K}$ is the reaction path curvature at the saddle point:

$$\mathbf{K} = \frac{\mathbf{H}^{(1)}\mathbf{Q}_{rxn} - [\mathbf{Q}_{rxn}^{T}\,\mathbf{H}^{(1)}\mathbf{Q}_{rxn}]\mathbf{Q}_{rxn}}{2\,[\mathbf{Q}_{rxn}^{T}\,\mathbf{H}^{(1)}\mathbf{Q}_{rxn}]\mathbf{I} - \mathbf{H}} \tag{43}$$

In (43) $\mathbf{H}^{(1)}$ is the first derivative of the Hessian at $s = 0$. While conventional methods usually take the first step along $\mathbf{Q}_{rxn}$, neglecting the second term in (42), here one steps along the actual curved path. This is important, if one is interested in properties sensitive to the reaction path curvature. In the commonly used approach these properties are not described correctly as the saddle point is approached.

The algorithm proposed by Page and McIver was recently applied by Koseki and Gordon [82] to successfully map the reaction path for the singlet SiH_2 inversion. The potential energy surface for this reaction is very flat and, as demonstrated by these authors, conventional gradient following methods do not yield reasonable paths.

Another, very different, approach to calculating the reaction path was

recently proposed by Jasien and Shepard [83]. This approach involves a reaction path-surface fitting cycle. Starting from a simple initial reference curve, e.g., a line connecting reactants, saddle point, and products, energies and gradients in the vicinity of the initial reference curve are evaluated and a fit of the surface is obtained. From this initial fit a steepest descent path is calculated. This path then becomes the new reference curve and additional energies and gradients in the vicinity of this curve are computed; this yields a new surface to use in determining the reaction path. As the fit is refined, the approximate surface approaches the true surface in the vicinity of the reaction path and the computed steepest descent path approaches the true reaction path. Using this strategy the new points at which to perform electronic structure calculations are selected in a systematic way, which makes this procedure attractive for computationally expensive high quality *ab initio* calculations. In most cases this procedure is expected to converge rapidly.

4. REACTION VALLEYS ON MOLECULAR POTENTIAL ENERGY SURFACES AND THE REACTION PATH HAMILTONIAN APPROACH

While valuable insights into the mechanism of a chemical reaction can be gained by determining the changes in the molecular structure along the reaction path, additional information is required for a detailed description of the dynamics of the reaction. To this end we will now explore and characterize the *reaction valley* leading from reactants through the saddle point to products, i.e., the $(3N-7)$-dimensional valley centered on the reaction path. In order to do so we have to define an appropriate coordinate set, a *natural reaction coordinate set*, where one of the coordinates describes motion along the path and the other coordinates describe the remaining degrees of freedom.

The idea of characterizing a reacting system by a natural coordinate set has frequently arisen in chemistry. In 1963 Hofacker [84] in his quantum theory of chemical reactions introduced the idea of describing a reacting system by a coordinate related to the progress of the reaction and the degrees of freedom perpendicular to this coordinate. Based on these ideas, Fischer et al. [85] derived a model approach to nonadiabatic reaction processes, and Hofacker and Levine [86] presented a nonadiabatic model for population inversion in molecular collisions. Fischer and Ratner [87] used the natural

coordinate set approach to derive a theory of translational–vibrational energy transfer for reactive collisions.

In 1966 Marcus [88] presented one of the first quantum mechanical scattering models for collinear A + BC reactions. In doing so, he introduced a set of coordinates that described the system point by point on a reaction path (being defined as a curve where the classical local vibrational and internal centrifugal forces balance) together with a distance vector from that point. He later extended this model to the three-dimensional case. The corresponding coordinates were referred to as *natural collision coordinates*. These coordinates played a dominant role in the first adiabatic calculations of quantum mechanical tunneling through the barrier of a potential energy surface.

In transition state theories (TST) [89], rate constants are obtained by calculating the flux through a surface dividing reactants from products. In conventional transition state theory [90] the location of the dividing surface is assumed to be perpendicular to the reaction coordinate at the saddle point, i.e., at $s = 0$. The system is then described by the reaction coordinate along with the bound vibrational modes. Together these define a natural coordinate set that we will call the reaction path coordinate set. In variational TST introduced by Truhlar and co-workers [91] the location of the bottleneck is varied along the reaction path in order find the point at which the flux is a minimum. Since the rates obtained from classical TST are upper bounds on the exact classical flux, this (normally) yields more accurate reaction rates than those obtained from conventional TST. Going beyond statistical approximations, semiclassical perturbation theories have been developed, e.g., the semiclassical perturbation-infinite order sudden approximation (SCP-IOS) [92], again based on a reaction path coordinate set. This model behaves qualitatively correctly both in the adiabatic limit, where the transverse vibrational motion is assumed to be much faster than motion along the reaction path, as well as in the sudden limit, where motion along the reaction path is assumed to be much faster than motion perpendicular to it.

In addition to its use in scattering theory and dynamics, the idea of a natural coordinate set has also been applied to problems in organic and inorganic chemistry. For example, Russegger and Brinkmann [93] described the pseudorotation of trigonal bipyramidal molecules (Berry rotation) in terms of a model using an internal reference coordinate corresponding to a fixed reference configuration and displacement coordinates perpendicular to it. A related problem arises in vibrational–rotational

spectroscopy if one of the internal coordinates undergoes large amplitude motions and can therefore no longer be described by standard vibrational-rotational theory. For such problems Hougen et al. [94] developed a model description that treats the large amplitude mode apart from all the other internal coordinates.

4.1 The Reaction Path Hamiltonian Approach

In 1980 Miller et al. [95] derived the Hamiltonian for a reacting molecular system which combined the early ideas of Hofacker and Marcus, the *IRC* of Fukui, and the large amplitude model of Hougen et al. This led in a straightforward fashion to a *reaction valley* description of the energetics and dynamics in polyatomic reactions. Miller et al. described the reacting system in terms of a reaction path coordinate set being composed of the reaction coordinate $\mathbf{x}_s(s)$ and the $(3N-7)$ local normal modes $\{\mathbf{Q}_k(s)\}$, obtained by diagonalizing the Hessian matrix at the point s on the reaction path. The Hessian matrix is constructed in the usual fashion except that the reaction coordinate is projected out (as before, there are also six zero frequency modes corresponding to overall translation and rotation). In terms of the coordinates $(\mathbf{x}_s, \{\mathbf{Q}_k\})$ and their conjugated momenta $(\mathbf{p}_s, \{\mathbf{P}_k\})$ the molecular Hamiltonian $\mathcal{H}(\mathbf{x}_s,\mathbf{p}_s,\{\mathbf{Q}_k\},\{\mathbf{P}_k\})$ is defined by

$$\mathcal{H}(\mathbf{x}_s,\mathbf{p}_s,\{\mathbf{Q}_k\},\{\mathbf{P}_k\}) = \mathcal{T}(\mathbf{x}_s,\mathbf{p}_s,\{\mathbf{Q}_k\},\{\mathbf{P}_k\}) + \mathcal{V}(\mathbf{x}_s,\{\mathbf{Q}_k\}) \tag{44}$$

In the approach of Miller et al. [95], the potential energy is approximated at each point s by the potential energy V_0 at that point on the path plus the potential energy for harmonic displacements perpendicular to the path:

$$\mathcal{V}(\mathbf{x}_s,\mathbf{Q}) = V_0\,[\mathbf{x}_s(s)] + \frac{1}{2}\sum_{k=1}^{3N-7} \omega_k(s)^2 Q_k(s)^2 \tag{45}$$

The kinetic energy is given by (for zero total angular momentum):

$$\mathcal{T}(\mathbf{x}_s,\mathbf{p}_s,\{\mathbf{Q}_k\},\{\mathbf{P}_k\}) = \frac{1}{2}\frac{\left[p_s - \sum_{k=1}^{3N-7}\sum_{k'=1}^{3N-7} B_{kk'}(s)Q_k(s)P_{k'}(s)\right]^2}{\left[1 - \sum_{k=1}^{3N-7} B_{ks}(s)Q_k(s)\right]^2} + \frac{1}{2}\sum_{k=1}^{3N-7} P_k(s)^2 \tag{46}$$

There are two different types of terms in the reaction path Hamiltonian that explicitly depend on the potential energy surface:

1. *The shape terms:* $x_S(s)$, $V_0(s)$ and $\{\omega_k(s)\}$. The shape of the reaction valley leading from reactants over the barrier to products is characterized by the reaction path $x_S(s)$, which determines the meandering of the floor of the reaction valley, the classical potential energy $V_0(s)$, which determines the height of the path, and the vibrational frequencies $\{\omega_k(s)\}$, which define the width of the valley (low frequencies denote a wide valley, high frequencies a narrow valley).
2. *The coupling terms,* $\{B_{ks}(s)\}$ and $\{B_{kk'}(s)\}$. As we shall see, these terms play an important role in the description of the reaction dynamics. They reflect the dynamic coupling between motion along the path and the transverse vibrations. It is through these terms that energy flows *non*adiabatically from translation to vibration and vice versa, $\{B_{ks}(s)\}$, and among the vibrations, $\{B_{kk'}(s)\}$.

4.2 The Terms in the Reaction Path Hamiltonian

From an analysis of the terms in the reaction path Hamiltonian, it is possible to provide a rationale for a variety of qualitative features of reaction dynamics.

The vibrationally adiabatic potentials describe the effect of vibrational energy on the reaction. They are obtained by adding the change in the vibrational energy, $\Delta E^v_{vib}(s)$ to the classical potential $V_0(s)$:

$$V^v_{vap}(s) = V_0(s) + \Delta E^v_{vib}(s) \tag{47}$$

where the vector v denotes the vibrational state (v_1, v_2, ...) of interest. In the harmonic approximation $\Delta E^v_{vib}(s)$ is simply

$$\Delta E^v_{vib}(s) = \sum_{k=1}^{3N-7} (v_k + \tfrac{1}{2})\hbar\,[\omega_k(s) - \omega_k(-\infty)] = \sum_{k-1}^{3N-7} (v_k + \tfrac{1}{2})\hbar\Delta\omega_k(s) \tag{48}$$

For v = (0, 0, ... 0), $V^0_{vap}(s)$ is the ground state adiabatic potential and $\Delta E^0_{vib}(s)$ is the zero point energy of the system at point s relative to that of the reactants ($s = -\infty$). If the frequency of one (or more) of the modes

decreases substantially during the course of the reaction, as would be expected, e.g., if a bond is broken, then $\Delta\omega_k$ will be negative and vibrational excitation for that mode will lead to a reduction in the vibrationally adiabatic barrier for the reaction and a corresponding increase in the reaction rate.

In order to calculate the vibrationally adiabatic potentials, the vibrational energy levels of the reactants and the saddle point must be properly correlated. Of course, one can just use the vibrational energies obtained as described above. Since the frequencies are obtained from a single Hamiltonian, they obey a noncrossing rule, i.e., frequencies corresponding to modes of the same symmetry do not cross. This is the *adiabatic* approximation. However, for many chemical reactions, like the OH + H_2 reaction discussed in the next section, a vibrationally *nonadiabatic* (or *diabatic*) model is more appropriate.

To properly correlate the vibrational levels we must consider the $B_{kk'}(s)$ coupling terms that are simply the dot product between the change of eigenvector $\mathbf{L}_k$ corresponding to normal mode k and the eigenvector $\mathbf{L}_{k'}$ corresponding to normal mode k' [96]:

$$B_{kk'}(s) = \frac{\partial \mathbf{L}_k(s)}{\partial s} \mathbf{L}_{k'}(s) \tag{49}$$

where ($\mathbf{L}_k(s)$; k = 1, $3N$–7) are the eigenvectors of the mass-weighted, projected Hessian matrix along the reaction path. The $B_{kk'}(s)$ terms describe the mixing between modes k and k' induced by motion of the system along the reaction path. As this motion involves a twisting of the vibrational modes about the reaction path, the $B_{kk'}(s)$ terms are referred to as *coriolis couplings*. The adiabatic model is rigorously valid only if all of the $B_{kk'}$ values are zero and hence there is no interaction between the transverse modes. Their character is then preserved during the course of the reaction and the vibrational modes can be trivially connected from reactants through the transition state to products. If there are nonzero values of $B_{kk'}(s)$, especially in the case of avoided crossings where the $B_{kk'}(s)$ values are large and localized, energy can readily flow from mode k to mode k'.

Translational–vibrational energy transfer during the course of the reaction is also a topic of considerable interest. The $B_{ks}(s)$ term is the dot product between the change in the eigenvector $\mathbf{L}_k$ and the reaction path $\mathbf{x}_s$

$$B_{ks}(s) = \frac{\partial \mathbf{L}_k(s)}{\partial s} \mathbf{x}_s(s) \tag{50}$$

It describes the dynamic coupling between the reaction path and vibrational mode k. It is a measure of the mixing between translational motion, i.e., motion along the reaction path, and vibrational motion in mode k induced by the curvature of the reaction path in the $(3N-6)$-dimensional space. As $B_{ks}(s)$ becomes larger, the mixing between the reaction path and vibration mode k increases and energy transfer from translation to vibration and vice versa becomes more and more facile. The total curvature of the reaction path is defined as

$$\kappa(s) = \left[\sum_{k}^{3N-7} B_{ks}(s)\right]^{1/2} \tag{51}$$

The $B_{ks}(s)$ terms are referred to as *curvature couplings.*

If a reaction is vibrationally adiabatic, the reaction path must have zero curvature, i.e., there must be no coupling between motion along the path and motion in the vibrational modes, $\{Q_k\}$, either from reactants to the transition state or from the transition state to products. In this case an exothermic reaction would convert all of the reaction energy into kinetic energy. This, however, does not apply to most chemical reactions. For these reactions nonadiabatic effects, i.e., the dynamic coupling between the motion along s and the motion along the $\{Q_k\}$ caused by the curvature of the reaction path, must be explicitly taken into account. Translational to vibrational energy transfer during the course of a reaction occurs in regions where $\kappa(s)$ is large. In the entrance channel, modes which have large $B_{ks}(s)$ values are *donating* modes, i.e., vibrationally excitation of these modes will cause energy to flow into the reaction path and, hence, the rate of reaction will be enhanced by having energy in this mode. In the exit channel, modes with large $B_{ks}(s)$ values are *accepting* modes. The reaction exoergicity can flow from the reaction path into these modes and lead to vibrational excitation of the products.

The curvature terms are intimately related to the well known propensity rules for abstraction reactions, in particular the rules put forward in the late 1960s by Polanyi and co-workers [97]. Polanyi and co-workers found that, for saddle points located in the exit channel, vibrational energy was far more effective than translational energy in overcoming the barrier to reaction. In this case the curvature is expected to be large before the saddle point is reached. Translational energy will then be efficiently drained into the transverse vibrational modes and, thus, not usable for surmounting the

Table 1. Relationship between Reaction Path Properties and Chemical Reaction Dynamics

Reaction path property		*Feature of reaction dynamics*
Classical potential	$V_0(s)$	Reaction rates in VTST [91]
Moment of inertia tensor	$I_s(s)$	
Vibrational frequencies	$\{\omega_k(s)\}$	
Normal modes	$\{Q_k(s)\}$	
Curvature couplings	$\{B_{ks}(s)\}$	Propensity rules for chemical reactions [97]
		Tunneling effects [99]
		Vibrational mode specificity in state selected decompositions[a]
		Vibrational mode specific enhancement of reaction rates[b]
		Prediction of product vibrational state distributions[b]
Coriolis couplings	$\{B_{kk'}(s)\}$	Correlation of reactant and product vibrational modes[b]
		Prediction of vibrationally enhanced product state distributions[b]

[a] Waite, B. A.; Miller, W. H. *J. Chem. Phys.* **1982**, *76*, 2412.
[b] See Section 4.

barrier. Vibrational energy in the modes strongly coupled to the reaction path, on the other hand, will be transformed into translational motion along the reaction path and hence provide the energy needed to overcome the barrier. When large curvatures are found on the product side, just the opposite is true. Translational energy can be directly used to overcome the barrier while vibrational energy will be ineffective. The details, of course, depend on the magnitudes and variations of the curvature coupling terms, $B_{ks}(s)$.

Within the framework of variational TST is it has been shown that the curvature of the reaction path, and hence the coupling terms, strongly influence quantum mechanical tunneling through the barrier [98]. The larger the coupling terms, the more facile tunneling is. There is a growing number of dynamic studies of polyatomic systems based on the RPH approach that has been reviewed recently [99].

In Table 1, the relationship between reaction path properties and dynamics is summarized. In the following section we will apply these ideas to the OH + H_2 reaction.

5. APPLICATION OF THE REACTION VALLEY APPROACH: THE OH + H_2 REACTION

There are few cases for which extensive dynamical studies have been carried out for a polyatomic system—one such series has been reported for the OH + H_2 reaction [100]. These studies include trajectory calculations by Schatz [101] as well as variational transition state theory calculations by Truhlar and Isaacson [102]. These studies rather thoroughly characterized the dynamics of the OH + H_2 reaction: determining the temperature dependence of the rate constant and the kinetic isotope effect, investigating the effect of translational, rotational, and vibrational excitation of the reactants on the reaction rate, and predicting the product state translational, rotational, and vibrational distributions. Both of these studies were based on an analytic potential energy surface developed by Schatz and Elgersma from the *ab initio* calculations of Walch and Dunning [103].[3] Dunning et al [80] calculated the terms in the reaction path Hamiltonian for this potential surface, characterizing the reaction valley from reactants through the saddle point to products. Here we will discuss the results of Schatz and co-workers and Isaacson and Truhlar in light of the analysis given in the previous section [105].

The classical potential along the reaction path for the OH + H_2 reaction obtained from the Schatz–Elgersma–Walch–Dunning potential energy surface is plotted in Figure 1. The height of the classical barrier is 6.1 kcal/mol while the reaction energy defect is predicted to be –15.2 kcal/mol. The barrier height for a chemical reaction is determined by a number of factors, including (1) ease with which the bond pair is transferred from the reactants to the products [83], (2) energy defect of the reaction [106], and (3) spin-exchange losses or gains [107]. The OH + H_2 reaction is a simple hydrogen transfer reaction in which formation of the new bond occurs simultaneously with the breakage of the old bond and, thus, the barrier is expected to be only a small fraction of the H_2 bond energy (the bond being broken). The OH + H_2 reaction is also very exoergic; barriers to reaction tend to decrease with increasing exoergicity.

To illustrate the spin-exchange effect, let us compare the barrier heights for the O + H_2 and OH + H_2 reactions. The barrier for the O + H_2 reaction

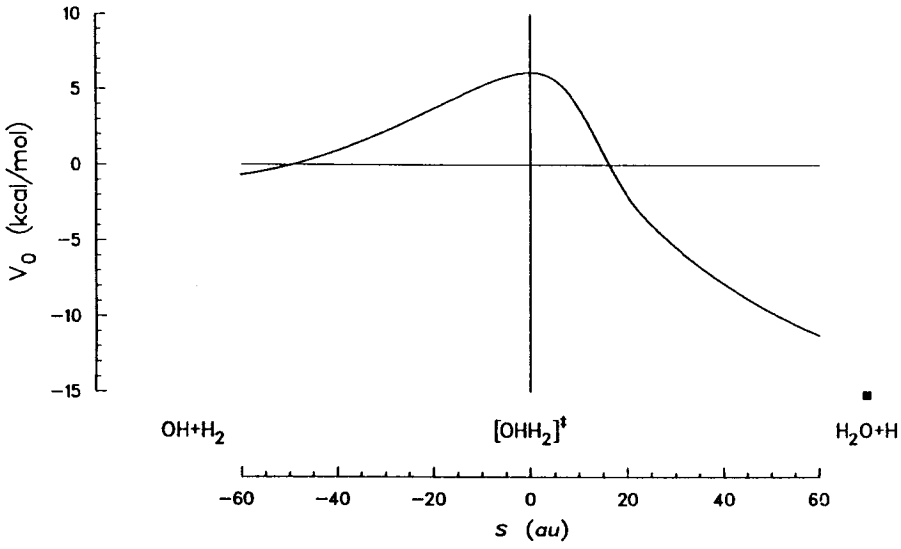

Figure 1. Classical potential for the OH + H_2 reaction along the reaction path. The black square denotes the calculated energy defect for the reaction.

is 12–13 kcal/mol. This barrier is significantly higher than that for OH + H_2 because the formation of the OH bond in the O—H_2 complex results in the partial loss of the exchange energy between the triplet coupled p-orbitals in the oxygen atom; there is no such loss in the HO—H_2 complex. The loss of exchange energy will continue to increase until the products have been formed. Using this model, Harding and Goddard [107] showed that the bond energies in the O—H and H—OH species are simply related by

$$\Delta D = D(\text{H–OH}) - D(\text{O–H}) \approx \tfrac{1}{2}K$$

where K is the exchange integral between the singly occupied p-orbitals in the oxygen atom. Averaging over the J manifolds for the lowest two LS states in the oxygen atom [108], one obtains K = 22.6 kcal/mol. Thus, the difference between the O—H and H—OH bond energies is predicted to be 11.3 kcal/mol; experimentally, the difference is 16.0 kcal/mol. Since the barrier heights for the O + H_2 and OH + H_2 reactions differ by 6–7 kcal/mol, this suggests that approximately one-half of the exchange energy contribution to ΔD is lost by the time the saddle point is reached (ignoring, of course, the differences in the relative positions of the saddle points).

The structure of the HOH_2 complex at selected points along the path are plotted in Figure 2. The hydroxyl radical can be considered a pseudo-halogen atom with the singly occupied π-orbital behaving much like the singly occupied *p*-orbital in the halogen atoms. The geometry of the saddle point is consistent with this, i.e., the oxygen atom and the two hydrogen atoms in the H_2 moiety are nearly collinear.[4] In addition, the saddle point is *early*, i.e., the length of the OH bond at the saddle point relative to its length in the product (H_2O),

$$\Delta R_{OH} = R_{OH}^{sp} - R_{OH}^{H_2O} = 0.26\text{Å}$$

is substantially larger than the change in the H_2 bond length from the reactants to the saddle point

$$\Delta R_{HH} = R_{HH}^{sp} - R_{HH}^{H_2} = 0.11\text{Å}$$

While the above provides welcome insights into the mechanism of the OH + H_2 reaction, we must determine the changes in the vibrational frequencies, $\{\omega_k(s)\}$, along the reaction path before we can predict the rate of the reaction. The calculated frequencies for the OH + H_2 reaction are plotted in Figure 3 and the normal modes at the saddle point are plotted in Figure 4 (the vibrational modes in the reactants and products are the familiar stretching and bending modes of OH, H_2 and H_2O). As is evident in both Figures 3 and 4, the OH stretching mode is little affected by reaction, the harmonic frequency decreasing by less than 100 cm^{-1} from reactants to the saddle point and increasing again by only slightly over 400 cm^{-1} from the saddle point to products. This mode correlates with the asymmetric stretching mode in H_2O (OH_{as}). The H_2 frequency, on the other hand, drops by over 2300 cm^{-1} from reactants to the saddle point, reaching a minimum of 1390 cm^{-1} at $s = 9$ au. The frequency of this mode then rises as the OH bond in H_2O is formed; this mode evolves into the symmetric stretching mode in H_2O (OH_{ss}). The remaining vibrational modes of the HOH_2 complex, ω_3, ω_4, and ω_5, correlate with rotations in the reactants. The mode corresponding to ω_3 correlates with the HOH bending mode in H_2O (HOH_b), while ω_4 and ω_5 correlate with rotations in the products.

Using the above data and variational transition state theory, Truhlar and Isaacson [102] calculated a rate constant for the OH + H_2 reaction of 10.5×10^{-15} cm^3/molec·sec at 298 K and 1.36×10^{-12} cm^3/molec·sec at 1000 K. The calculated rate constants are in good agreement with the measured

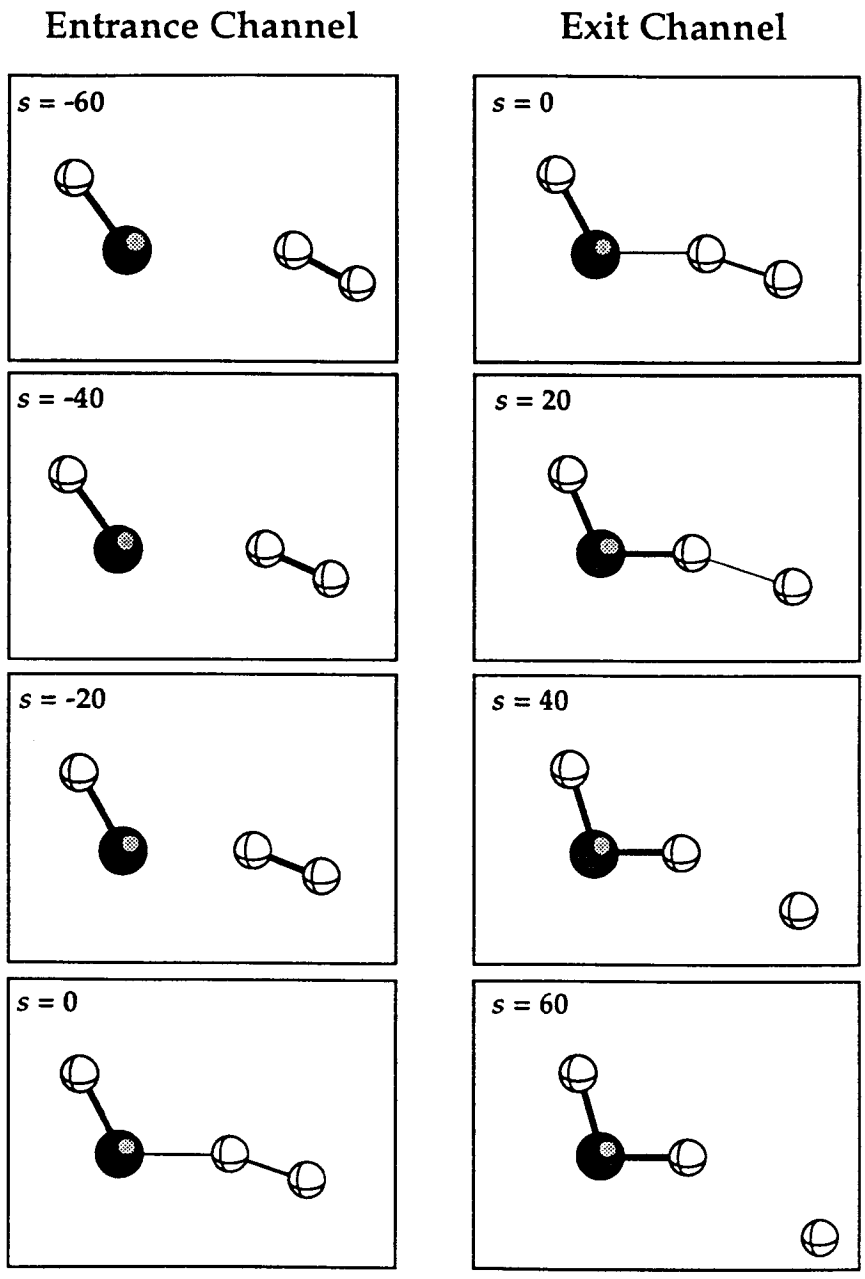

Figure 2. Structure of the OHH_2 complex at selected points along the reaction path. The oxygen atom is presented by the dark sphere and the hydrogen atoms by white spheres.

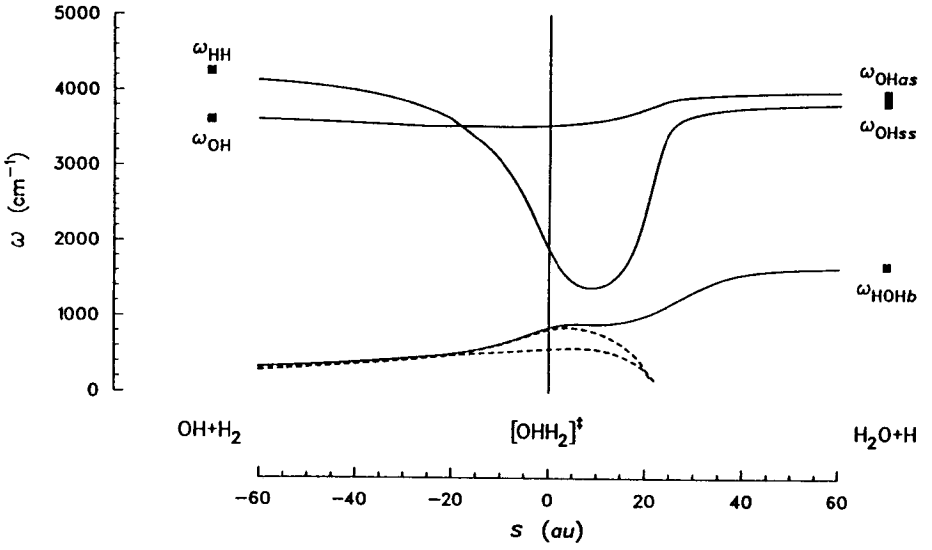

Figure 3. Vibrational frequencies along the reaction path for the OH + H_2 reaction. The dashed curves correspond to the in-plane and out-of-plane wagging modes. The black squares denote the calculated vibrational frequencies for the reactants and products.

values: 6.08×10^{-15} cm^3/molec·sec at 298 K and 1.99×10^{-12} cm^3/molec·sec at 992 K [109].

The vibrationally adiabatic potentials for the ground state, (v_{OH}=0, v_{H_2}=0), and the two vibrationally excited states, (v_{OH}=1, v_{H_2}=0) and (v_{OH}=0, v_{H_2}=1), are plotted in Figure 5. The ground state vibrationally adiabatic potential at s = 0, 5.9 kcal/mol is only slightly lower than the classical barrier height, 6.1 kcal/mol. The 6.7 kcal/mol drop in the H_2 stretching frequency from reactants to the saddle point is largely offset by the growth in the frequencies of modes which build-in as the reaction proceeds: the HOH bending mode (ω_{HOH_b} = 857 cm^{-1}), the in-plane wagging mode (ω_4 = 572 cm^{-1}), and the out-of-plane wagging mode (ω_5 = 829 cm^{-1}). Note, however, that the maximum in the adiabatic potential, 6.2 kcal/mol, is at s = –5, not at the saddle point. Vibrational excitation of the OH molecule decreases the vibrationally adiabatic threshold by only 0.3 kcal/mol while excitation of the H_2 molecule decreases the threshold by 3.0 kcal/mol. Thus, vibrational excitation of the OH species would be expected to have a negligible effect on the rate of the reaction, whereas the effect of

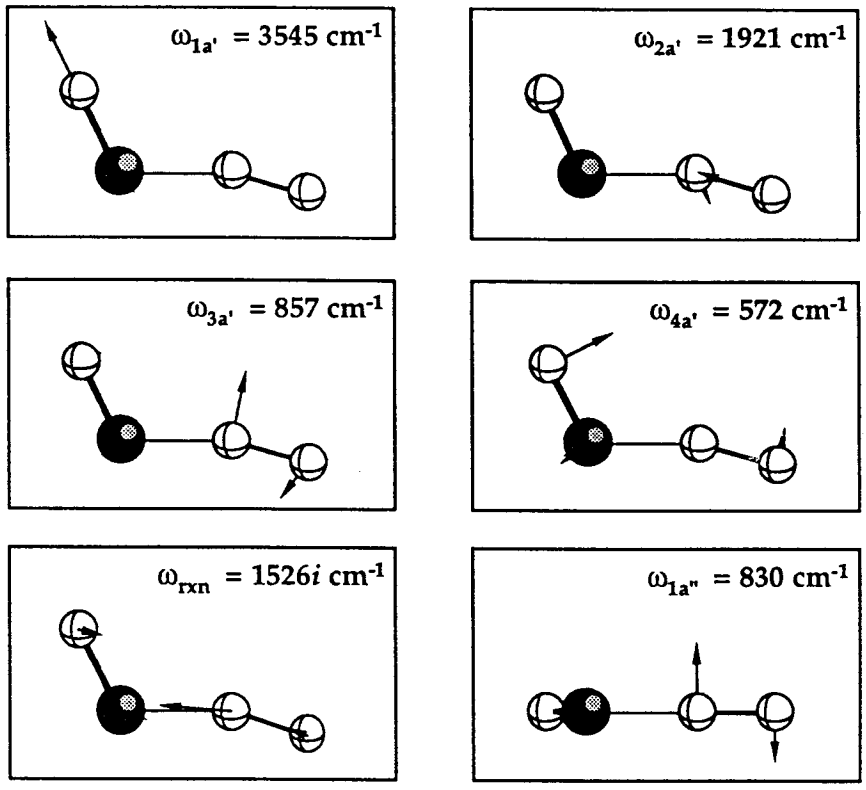

Figure 4. Vibrational modes of the OH+H_2 complex at the saddle point. The reaction coordinate is associated with ω_{rxn}. The oxygen atom is represented by a dark sphere and the hydrogen atoms by white spheres. The lengths of the displacement vectors have been multiplied by 1.5 for display.

vibrationally exciting the H_2 would be substantial. Even in the latter case, however, vibrational excitation is relatively inefficient in accelerating the rate of the reaction—the barrier is decreased by only a quarter of the vibrational quanta in H_2.

Both Schatz [101] and Truhlar and Isaacson [102] have reported dynamic calculations of the effect of vibrational excitation on the rate of the OH + H_2 reaction. The variational transition state theory calculations of Truhlar and Isaacson [102] predicted an enhancement of a factor of 108 in the reaction rate for vibrationally excited H_2 and of 1.58 for reaction with vibrationally excited OH. At 300 K they found that vibrational excitation

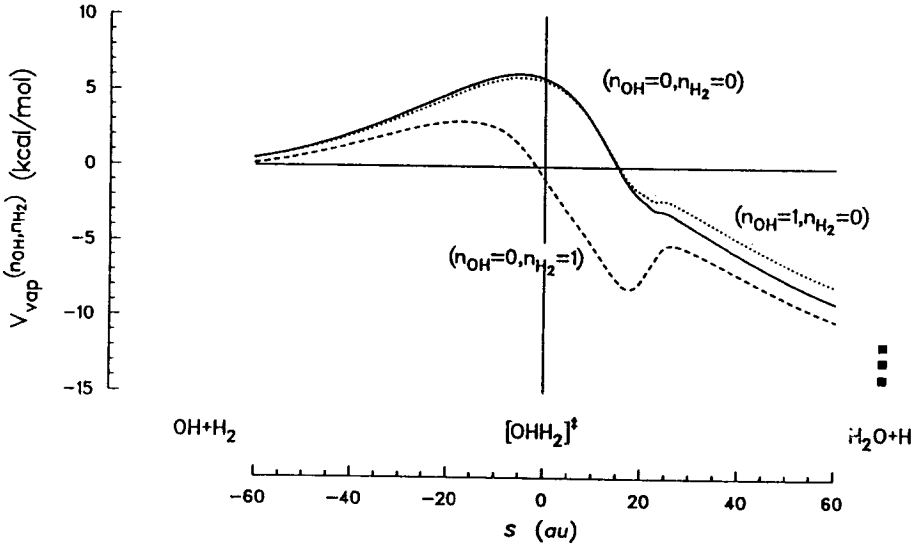

Figure 5. Vibrationally adiabatic potentials, $V^{(\nu_{OH},\nu_{H_2})}$ for the $OH(\nu_{OH})$ + $H_2(\nu_{H_2})$ reaction. The black squares denote the calculated exoergicities of the reactions.

of H_2 decreased the activation energy by 2.5 kcal/mol and increased the preexponential term by a factor of 1.6. Schatz [101] reported a reduction of 3.4 kcal/mol in the threshold for reaction with vibrationally excited H_2. He predicted a rate constant at 300 K for $H_2(\nu_{H_2} = 1)$, which was a factor of 390 larger than that for $H_2(\nu_{H_2} = 0)$. Vibrational excitation of the OH radical, on the other hand, led to a negligible enhancement in the rate (only a factor of 1.28).

These results agree well with the experimental data available for the vibrationally enhanced reactions. Zellner and Steinert [110] report a rate enhancement for H_2 ($\nu_{H_2} = 1$) of a factor of 120 ± 40 at 300 K, while Glass and Chaturvedi [111] report a factor of 155 ± 38. Further, based on preliminary measurements of the temperature dependence of the rate of OH + H_2, Zellner and Steinert estimated a decrease of 3.4 kcal/mol in the activation energy for reaction with vibrationally excited H_2; this compares well with the calculated reductions in the thresholds. In contrast, Spencer et al. [112] found that vibrational excitation of OH increased the OH + H_2 reaction rate by less than a factor of two, in line with the theoretical predictions. (See also [113].)

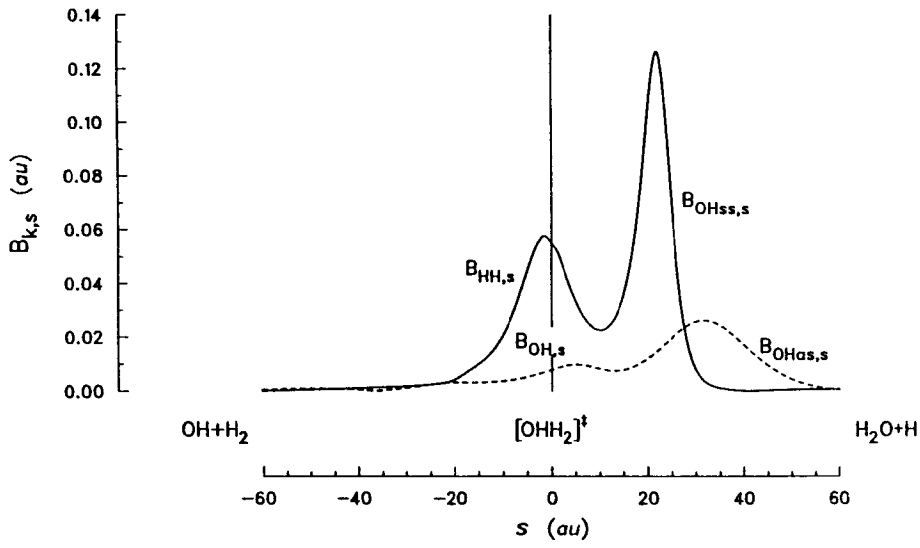

Figure 6. Curvature coupling terms for the H_2 (OH_{ss}) and OH (OH_{as}) modes along the reaction path for the OH + H_2 reaction.

As seen in Section 3, the reaction path Hamiltonian contains, in addition to the vibrational frequencies and normal modes, the terms coupling motion along the path with the vibrational motions transverse to the path, $\{B_{ks}(s)\}$, and the terms coupling the vibrational motions induced by motion along the path, $\{B_{kk'}(s)\}$. These terms govern the *non*adiabatic flow of energy between the bound modes and the reaction coordinate. Although the detailed influence of the coupling terms on the reaction can be determined only from dynamics calculations, important insights into vibrational effects in chemical reactions can be obtained from an examination of these terms alone [114]. As can be seen in Figure 6, there is almost no coupling between the OH stretch and the reaction path in the entrance channel; the value $B_{OH,s}$ is nearly zero there. Thus, there is no way for the vibrational energy to flow into the reaction path. This is, of course, expected given the minor changes in $\omega_{OH}(s)$ noted in Figure 3. The OH bond is simply a *spectator bond.* The H_2 stretching mode, on the other hand, strongly couples with the reaction path in the entrance channel with $B_{HH,s}$ attaining a maximum value just before the saddle point in the entrance channel. Energy can flow nonadiabatically from the H_2 stretch into the reaction path via the $B_{HH,s}$ coupling term, and, hence, excitation of this bond has a substantial effect on the reaction rate.

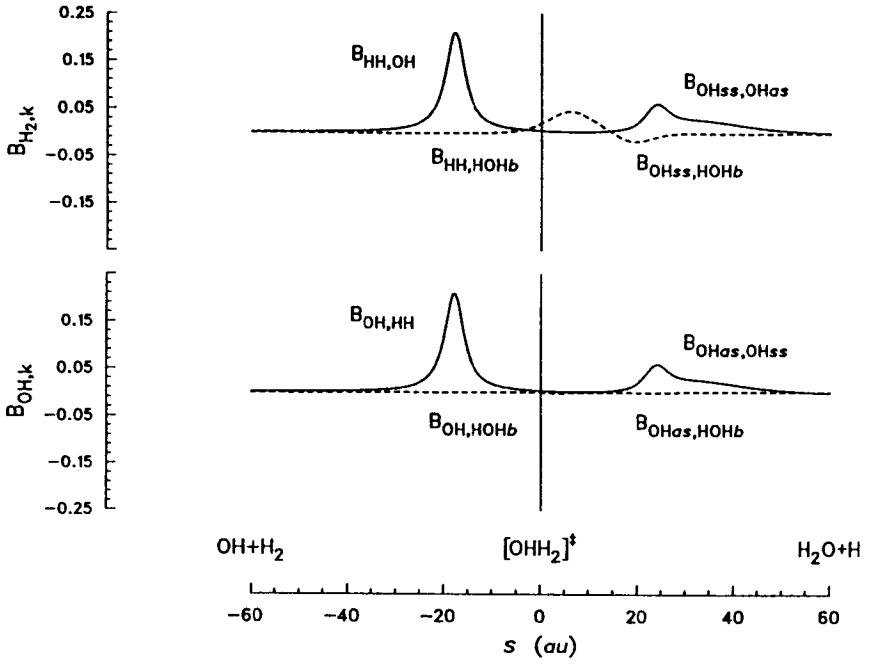

Figure 7. Coriolis coupling terms for the (OH_{ss}) and OH (OH_{as}) modes along the reaction path for the OH + H_2 reaction.

Within the framework of the reaction path Hamiltonian approach, frequencies of the same symmetry do not cross. In the present case, the mode that correlates with the H_2 stretching mode (at 4260 cm^{-1}) drops in frequency as the saddle point is approached, while the mode which correlates with the OH stretching mode (at 3620 cm^{-1}) is largely unaffected. There is an avoided crossing of these two curves just before the saddle point, at $s \approx -18$ au. In Figure 7 we plot the coriolis terms coupling the H_2 and OH stretching and HOH bending modes. As outlined in Section 3, coriolis coupling terms are expected to be large in the vicinity of a sharply avoided crossing. In fact, in the entrance channel, there is essentially no coupling between the OH and the H_2 stretch except in the vicinity of the avoided crossing. At that point there is a sharp peak in the $B_{OH,HH}$ term, which will induce a localized (diabatic) transition between the two adiabatic states. Hence, we conclude that it is physically more reasonable to assume that the OH and H_2 stretches preserve their character during the course of the reaction. Knowing this, we

plotted the vibrational frequencies in Figure 3 as if the curves for $\omega_{OH}(s)$ and $\omega_{H_2}(s)$ do in fact cross. The same assumption was also used to compute the vibrationally adiabatic potentials plotted in Figure 5.

The influence of vibrational excitation on the product state distribution yields further insights into the dynamic of chemical reactions [115]. In his quasiclassical trajectory study, Schatz [101] found that for both vibrationally excited OH and H_2 the excess energy is deposited preferentially in the H_2O vibrational degrees of freedom. Virtually no energy is transferred to product translational motion and very little to the rotational degrees of freedom. The distribution of the energy among the H_2O vibrational degrees of freedom is even more intriguing. For vibrationally excited H_2 Schatz observed a nonspecific distribution of the excess energy among the H_2O modes: 42% went into the symmetric stretch mode, 35% into the asymmetric stretch mode, and 22% into the bending mode. On the other hand, when the OH is initially excited, all of the excess energy goes into the OH stretching modes: 75% to the asymmetric stretch and 25% to the symmetric stretch. None of the excess energy flows into the bending mode.

While both trajectory calculations as well as experimental studies can determine the effect of vibrational excitation on a chemical reaction, they do not provide a rationale for it. However, the reaction valley approach presented here does! It provides a framework within which to understand why given state distributions are obtained. In Figure 3 we see that the H_2 mode evolves into the OH symmetric stretching mode (OH_{ss}) in H_2O. If the reaction were adiabatic, excitation energy in the H_2 mode would all be deposited in the OH_{ss} mode. However, as is seen in the upper panel in Figure 7, there are significant couplings between the H_2/OH_{ss} mode and the OH_{as} and HOH_b modes in the exit channel (as well as between this mode and the path). Thus, excitation energy in the H_2 mode can flow into all of the vibrational modes in the water product. The net result is a broad distribution of the vibrational excitation energy among the product stretching and bending modes. In contrast, there is little coupling between the OH stretch and the HOH bending mode (see lower panel in Fig. 7). The only important coupling is between the OH_{ss} and OH_{as} modes in the exit channel. In this case the vibrational excitation energy is confined to the OH stretching modes in the products, with little of the energy being deposited in the bending mode.

Finally, the reaction path analysis outlined here sheds light on the detailed dynamics of the reverse of reaction the OH + H_2 reaction, H + H_2O. In a classical trajectory study of this reaction, Elgersma and Schatz [116] and

Schatz and co-workers [117] found that the symmetric stretch mode of H_2O was far more efficient in enhancing the rate of the reaction than either the bending or asymmetric stretching modes. They found that the threshold for reaction was lowered by ~90% of the symmetric stretch vibrational quantum but only by ~70% and ~60% of the bending or asymmetric stretch quanta, respectively.

These observations seem to contradict chemical intuition. It might have been thought that the asymmetric stretch mode would most closely resemble the reaction coordinate and hence this mode should be strongly coupled with the reaction coordinate in the H + H_2O reaction. Again, the reaction path analysis resolves this puzzle. As is clearly evident in Figure 3, it is the symmetric stretch mode that is most strongly affected by reaction—its frequency drops from 3860 cm^{-1} in H_2O to 1920 cm^{-1} at the saddle point. The frequencies of the asymmetric stretch and bending modes change far less over this same region and, hence, are far less effective in accelerating the rate of reaction.

6. CONCLUSIONS

Chemists traditionally describe chemical reactions in terms of activation energies (barriers to reaction), preexponential factors (activation entropies), transition states (critical intermediate molecular configurations), and reaction paths (continuous evolution of reactants into products). Although much information on chemical reactions can be obtained from measurements of the rates, cross sections, angular distributions, etc., the transitory molecular species involved in chemical reactions are not directly amenable to experimental characterization—the time scales of chemical transformations are far too short to be observed by traditional chemical techniques (see [35] however). Thus characterization of the details of chemical reactions must rely on theory.

Within the past decade there have been a number of advances in the theoretical calculation and characterization of molecular potential energy surfaces, including the development of direct configuration interaction [118], many body perturbation theory, and coupled-cluster [119] techniques for computing accurate interaction energies and analytical techniques for computing the derivatives of the interaction energy [16,17]. With these new techniques, it is possible to locate and characterize stable and metastable molecular species (minima) and transition states (saddle points) for chemical reactions and to compute the paths connecting reactants with products

(*IRC*). These calculations provide quantitative information on reaction energetics and yield valuable insights into the mechanisms of chemical reactions (see, e.g., the chapter by L. Harding and references therein).

By characterizing the reaction valley, leading from reactants through the transition state to products, the features of the potential energy surface can be directly connected with the reaction dynamics. The reaction valley is characterized by the *shape* terms, $x_s(s)$, $V_s(s)$, and $\{\omega_k(s)\}$, which define the location and features (slope and width) of the valley, and by the *dynamic* terms, $\{B_{ks}(s)\}$ and $\{B_{kk'}(s)\}$, which describe the nonadiabatic flow of energy among the translational and vibrational degrees of freedom. Consideration of these terms provides a simple model for understanding much of the detailed dynamics of chemical reactions, including the effects of vibrational excitation of the reactants and vibrational distributions in the products, in terms familiar to chemists.

ACKNOWLEDGMENTS

One of the authors (E. K.) wishes to thank Professor Dieter Cremer for many helpful discussions. This work was supported by the Division of Chemical Sciences, Office of Basic Energy Research, U.S. Department of Energy under contract W-31-109-ENG-38.

NOTES

1. Present address: Institute für Organische Chemie, Universität Köln, Köln, Federal Republic of Germany.
2. We prefer to call the *IRC* the "Intrinsic Reaction Path" since the definition yields a curve in $(3N-6)$ space. The intrinsic reaction coordinate would then refer to the path tangent at any given point on the path; the reaction coordinate, of course, changes as one moves along the path. Unfortunately, the terminology in common use does not make this distinction.
3. Rasheed and Brown [104] also reported trajectory calculations on this reaction; however, they used a slightly modified version of the Schatz–Elgersma–Walch–Dunning potential surface.
4. The conformation of the saddle point predicted by Walch and Dunning [103] was *cis*; that predicted by the fitted surface is *trans*.

REFERENCES

1. Truhlar, D. G.; Steckler, R.; Gordon, M. *Chem. Rev.* **1987**, *87*, 217, and references therein.
2. Sathyamurthy, N. *Comp. Phys. Rep.* **1986**, *3*, 1, and references therein.

3. Carter, S. *Comp. Phys. Rep.* **1986**, *3*, 209.
4. Lawley, K. P. (ed.). *Potential Energy Surfaces*. New York: Wiley, 1980.
5. Dunning, T. H., Jr.; Harding L. B. In *Theory of Chemical Reaction Dynamics*, M. Baer (ed.). Vol. 1, p. 1. Boca Raton, FL: CRC Press, 1985.
6. Murrell, J. N.; Carter, S.; Farantos, S. C.; Huxley, P.; Varandas, A. J. C. *Molecular Potential Energy Functions*. New York: Wiley, 1984.
7. Truhlar, D. G. (ed.). *Potential Energy Surfaces and Dynamics Calculations*. New York: Plenum, 1981.
8. Murrell, J. N.; Laidler, K. L. *Trans. Faraday Soc.* **1968**, *64*, 371.
9. For a discussion of the topology of molecular potential energy surfaces see, e.g., (a) Mezey, P. G. *J. Mol. Struct. (Theochem.)* **1987**, *49*, 57. (b) Basilevsky, M. V. *Chem. Phys.* **1982**, *67*, 337. (c) Fernandez, A.; Sinanoglu, O. *Theor. Chim. Acta* **1984**, *65*, 179.
10. For a recent review of numerical methods for locating critical points on molecular potential energy surfaces, see Schlegel, B. H. *Adv. Chem. Phys.* **1987**, *67*, 249.
11. For a recent review on how to locate transition states see Bell, S.; Crighton, J. S. *J. Chem. Phys.* **1984**, *80*, 2464.
12. Fletcher, R. *Practical Methods of Optimization*. New York: Wiley, 1980.
13. Press, W. H.; Flannery, B. P.; Teukolsky, S. A.; Vetterling W. T. *Numerical Recipes, the Art of Scientific Computing*. New York: Cambridge University Press, 1986.
14. Gill,P. E.; Murray, W.; Wright, M. H. *Practical Optimization*. New York: Academic Press, 1982.
15. Powell, M. J. D. (ed.). *Non-linear Optimization*. New York: Academic Press, 1982.
16. For a recent review of analytical energy methods see Pulay, P. *Adv. Chem. Phys.* **1987**, *67*, 241.
17. *Geometric Derivatives of Energy Surfaces and Molecular Properties*. Jorgensen, P.; Simons, J. (eds.). Holland: Reidel, 1986.
18. See, e.g., Ref. [13], Chap. 9, and references therein.
19. See, e.g., Ortega, J.; Rheinboldt, W. *Iterative Solution of Nonlinear Equations in Several Variables*. New York: Academic Press, 1970.
20. See, e.g., Stoer, J.; Burlisch, R. *Introduction to Numerical Analysis*, Chap. 8. New York: Springer-Verlag, 1980.
21. See, e.g., Ref. [13], Chap. 10, and references therein.
22. For a recent discussion of determining the initial Hessian for gradient-type geometry optimization see Schlegel, H. B. *Theor. Chim. Acta* **1984**, *66*, 333.
23. Typical updating schemes are, for example, (a) the Broyden family of algorithms: Broyden, C. G. *Math. Comp.* **1967**, *19*, 368; or (b) the Huang family of algorithms: Huang, D. Y. *J. Opt. Theor. Appl.* **1970**, *5*, 405.
24. Fletcher, R.; Powell, M. J. D. *Comput. J.* **1963**, *6*, 163. Davidson, W. Argonne National Laboratory Report, ANL-5990, Argonne, IL, 1959.
25. Hoffmann, U.; Hofmann, H. *Einführung in die Optimierung*, Chap. 4. Weinheim: Verlag Chemie, 1971.
26. Murtagh, B.; Sargent, R. W. H. *Comput. J.* **1972**, *13*, 185.
27. Polak, E. *Computational Methods in Optimization*, Chap. 2. New York: Academic Press, 1971.
28. Fletcher, R.; Reeves, C. M. *Comput. J.* **1964**, *7*, 149.
29. Schlegel, H. B. *J. Comput. Chem.* **1982**, *3*, 214.
30. (a) McIver, J. W., Jr.; Komornicki, A. *J. Am. Chem. Soc.* **1972**, *94*, 2625. (b)

Kormornicki, A.; Ishida, K.; Morokuma, K.; Ditchfield, R.; Conrad, M. *Chem. Phys. Lett.* **1977**, *45*, 595.
31. (a) Simons, J.; Jorgensen, P.; Taylor, H.; Ozment, J. *J. Phys. Chem.* **1983**, *87*, 2745. (b) Banerjee, N.; Adams, N.; Simons, J.; Shepard, R. *J. Phys. Chem.* **1985**, *89*, 52.
32. (a) Algorithm for analytical gradients: Baker, J. *J. Comput. Chem.* **1986**, *7*, 385. (b) Algorithm for numerical gradients: Baker, J. *J. Comput. Chem.* **1987**, *8*, 563.
33. Cerjan, C. J.; Miller, W. H. *J. Chem. Phys.* **1981**, *75*, 2800.
34. See, e.g., Vilkovi, V.; Mastryukov, V. S.; Sadova, N. I. *Determination of the Geometrical Structure of Free Molecules.* Moscow: Mir Publishers, 1983.
35. For a recent discussion of laser probing of transition states see Zewail, A. H. *Science*, **1988**, *1645*.
36. See, e.g., Melander, L. C. S.; Saunders, W. H., Jr. *Reaction Rates of Isotopic Molecules.* New York: Wiley-Interscience, 1980.
37. See, e.g., Frost, A. A.; Pearson, R. G. Kinetics and Mechanism, 2nd ed. New York: Wiley, 1961.
38. Wilson E. B., Jr.; Decius, J. C.; Cross, P. C. *Molecular Vibrations.* New York: Dover, 1980.
39. See, e.g., Ref. [38], p. 193.
40. Truhlar, D. G.; Brown, F. B.; Steckler, R.; Isaacson, A. D. In *The Theory of Chemical Reaction Dynamics*, p. 285. New York: Reidel, 1986.
41. Müler, K. *Angew. Chem. Int. Ed. Engl.* **1980**, *19*, 1.
42. Walker, R. B.; Light, J. C. *Ann. Rev Phys. Chem.* **1980**, *31*, 401.
43. Basilevsky, M. V.; Ryaboy, V. M. *Chem. Phys.* **1980**, *50*, 231.
44. Badea, F. *Reaction Mechanisms in Organic Chemistry*, Chap. 12. Kent: Abacus Press, 1977, and references therein.
45. Rothman, M. J.; Lohr, L. L. Jr. *Chem. Phys. Lett.* **1980**, *70*, 405.
46. Burkert, U.; Allinger, N. L. *J. Comput. Chem.* **1982**, *3*, 40.
47. Williams, I. H.; Maggiora, G. M. *J. Mol. Struct.* **1982**, *89*, 365.
48. McCullough E. A., Jr.; Silver, D. M. *J. Chem. Phys.* **1975**, *62*, 4050.
49. Nauts, A.; Chapuisat, X. *Chem. Phys. Lett.* **1982**, *85*, 212. These authors ask to what extent a coordinate-free definition of the steepest descent can be given.
50. Sana, M.; Reckinger, G.; Leroy, G. *Theor. Chim. Acta* **1981**, *58*, 145. These authors show that the steepest descent path does not correspond to an invariant curve under coordinate transformation.
51. Quapp, W.; Heidrich, D. *Theor. Chim. Acta* **1984**, *66*, 245. These authors claim to have found a way to define a coordinate independent steepest descent path.
52. Fukui, K. J, *J. Phys. Chem.* **1970**, *74*, 4161; see also Fukui, K. *Acct. Chem. Res.* **1981**, *14*, 368.
53. (a) Hoffman, D. K.; Nord, R. S.; Ruedenberg, K. *Theor. Chim. Acta* **1986**, *69*, 265. (b) Jorgensen, P.; Jensen, H. J. A.; Helgaker, T. *Theor. Chim. Acta* **1988**, *73*, 55.
54. Shavitt, I. "The Tunnel Effect Corrections to the Rates of Reactions with Parabolic and Eckart Barrier." Report WIS-AEC-23, Theoretical Chemistry Laboratory, University of Wisconsin, Madison, WI, 1959. See also, Truhlar, D. G.; Kuppermann, A. *J. Am. Chem. Soc.* **1971**, *93*, 1840.
55. Eliason, M. A.; Hirschfelder, J. O. *J. Chem. Phys.* **1959**, *30*, 1426.
56. See, e.g., Yamashita, K.; Yamabe, T.; Fukui, K. *Chem. Phys. Lett.* **1981**, *84*, 123; Yamashita, K.; Yamabe, T.; Fukui, K. *Theor. Chim. Acta* **1982**, *60*, 523; Yamabe, T.; Koizumi, M.; Yamashita, K.; Tachibana, A. *J. Am. Chem. Soc.* **1984**, *106*, 2255.

57. See e.g., Goldstein, H. *Classical Mechanics*, 2nd ed. London: Addison-Wesley, 1980.
58. Eckart, C. *Phys. Rev.* **1937**, *47*, 552.
59. See, e.g., Laugwitz, D. *Differential and Riemannian Geometry*. New York: Academic Press, 1965.
60. See, e.g., (a) Tachibana, A.; Fukui, K. *Theor. Chim. Acta* **1978**, *49*, 321. (b) Tachibana, A.; Fukui, K. *Theor. Chem. Acta* **1980**, *57*, 81. (c) Tachibana, A.; Yamashita, K. *Int. J. Quant. Chem. Symp.* **1981**, *15*, 621. (d) Fukui, K. *Int. J. Quant. Chem. Symp.* **1981**, *15*, 633.
61. Igawa, A.; Fukutome, H. *Chem. Phys. Lett.* **1987**, *133*, 399.
62. Pearson, R. G. *Symmetry Rules for Chemical Reactions*. New York: Wiley, 1976.
63. Pick, S.; Friederich, B. *Collect. Czech. Chem. Com.* **1986**, *51*, 1171.
64. See, e.g., Yamabe, T.; Koizumi, M.; Yamashita, K.; Tachibana, A. *J. Am. Chem. Soc.* **1984**, *106*, 2255. Yamashita, K.; Yamabe, T. *Int. J. Quant. Chem. Symp.* **1983**, *17*, 177. Fukui, K.; Kato, S.; Fujimoto, H. J. *J. Am. Chem. Soc.* **1974**, *97*, 1.
65. See, e.g., the Li + HF reaction, described in Dunning, T. H., Jr.; Kraka, E.; Eades, R. A. *Faraday Discuss. Chem. Soc.* **1987**, *84*, 427.
66. See, e.g., Dunning, T. H., Jr.; Harding, L. B.; Bair, R. A.; Eades, R. A.; Shepard, R. *J. Phys. Chem.* **1986**, *90*, 344. Dunning, T. H., Jr. *J. Chem. Phys.* **1984**, *88*, 2469.
67. (a) Bobrowicz, F. W.; Goddard, W. A. III. In *Methods of Electronic Structure Theory*, H. F. Schaefer III (ed.), p. 79. New York: Plenum, 1977. (b) Goddard, W. A. III; Dunning, T. H., Jr.; Hunt, W. J.; Hay, P. J. *Acc. Chem. Res.* **1973**, *6*, 368.
68. Goddard, W. A. III. *J. Am. Chem. Soc.* **1971**, *94*, 793.
69. Page, M.; McIver, J. W., Jr. *J. Chem. Phys.* **1988**, *88*, 922.
70. Mass-weigthed Cartesian coordinates have units of $\sqrt{mass \times length}$ and are usually given as $\sqrt{u\,a_0}$ or $\sqrt{u}$ Å where 1 u = 1 universal (^{12}C) atomic mass unit = 1822.887 m_e and 1 a_0 = 1 bohr = 0.5291771 Å.
71. Kraka, E.; Dunning, T. H., Jr. to be published. Baldrige, K. K.; Schmidt, M. W.; Bartol, D.; Gordon, M. American Conference on Theoretical Chemistry, Gull Lake, Minnesota, 1987. See also Ref. [40].
72. Ishida, K.; Morokuma, K.; Kormornick, A. *J. Chem. Phys.* **1977**, *66*, 2153.
73. Schmidt, M. W.; Gordon, M. S.; Dupuis, M. *J. Am. Chem. Soc.* **1985**, *107*, 2585.
74. Müller, K.; Brown, L. D. *Theor. Chim. Acta* **1979**, *53*, 75.
75. Gonzales, C.; Schlegel, H. B. to be published; the method is briefly described in Ref. [10].
76. See LSODA—*Livermore Solver for Ordinary Differential Equations* (with and without method switching for stiff- and nonstiff problems), Petzold, L. R.; Hindmarsch, A. C. (Scandia National Laboratory, Livermore, CA, 1985).
77. See Forman, S. A. *Numerical Methods That Work*, Chap. 5. New York: Harper & Row, 1970.
78. Gear, W. C. *Numerical Initial Value Problems in Ordinary Differential Equations*. New York: Prentice Hall, 1971.
79. Kraka, E.; Dunning, T. H., Jr. to be published.
80. STEEP—*a computer code for calculating reaction paths*, Harding, L. B.; Kraka, E. Argonne National Laboratory, Argonne, 1987.
81. Pechukas, P. J. *Chem. Phys.* **1976**, *64*, 1516.
82. Koseki, S.; Gordon, M. S. *J. Phys. Chem.*, in press.
83. Jasien, P. G.; Shepard, R. *Int. J. Quant. Chem.* (to be published).

84. Hofacker, G. L. Z. *Naturforsch.* **1963**, *18a*, 607.
85. Fischer, S. F.; Hofacker, G. L.; Seiler, R. *J. Chem. Phys.* **1969**, *51*, 3951.
86. Hofacker, G. L.; Levine, R. D. *Chem. Phys. Lett.* **1971**, *9*, 617.
87. Fischer, S. F.; Ratner, M. A. *J. Chem. Phys.* **1972**, *57*, 2769.
88. Marcus, R. A. *J. Chem. Phys.* **1966**, *45*, 4493; **1966**, *45*, 4500; **1949**, *49*, 2610.
89. Truhlar, D. G.; Isaacson, A. D.; Garrett, B. C. In *Theory of Chemical Reaction Dynamics*, M. Baer (ed.), Vol. 4, p. 65. Boca Raton, FL: CRC Press, 1985.
90. Truhlar, D. G.; Hase, W. L.; Hynes, J. T. *J. Phys. Chem.* **1983**, *87*, 2664.
91. Truhlar, D. G. *Annu. Rev. Phys. Chem.* **1984**, *35*, 159.
92. (a) Miller, W. H.; Shi, S.-H. *J. Chem. Phys.* **1981**, *75*, 2258. (b) Miller, W. H.; Smith, F. T. *Phys. Rev.* **1978**, *A17*, 939.
93. Russeger, P.; Brickmann, J. *J. Chem. Phys.* **1975**, *62*, 1086.
94. Hougen, J. T.; Bunker, P R.; Johns, J. W. C. J. *J. Mol. Spectrosc.* **1973**, *45*, 120.
95. Miller, W. H.; Handy, N. C.; Adams, J. E. *J. Chem. Phys.* **1980**, *72*, 99.
96. An efficient evaluation of the coupling terms by use of gradients and force constants together with the components of the third derivatives along the reaction path tangent has recently been proposed in Ref. [69].
97. Polanyi, J. C.; Wong, W. H. *J. Chem. Phys.* **1969**, *51*, 1439. See also Polanyi, J. C. *Acc. Chem. Res.* **1972**, *5*, 161.
98. See, e.g., Miller, W. H. *Chem. Rev.* **1987**, *87*, 19. Skodje, R. T.; Truhlar, D. G. *J. Chem. Phys.* **1982**, *77*, 5955.
99. See, e.g., Miller, W. H. In *The Theory of Chemical Reaction Dynamics*, D. C. Clary (ed.), p. 27. Dordrecht: Reidel, 1986. Miller, W. H. *J. Phys. Chem.* **1983**, *87*, 3811. Truhlar, D. G.; Garrett, B. C. *Annu. Rev. Phys. Chem.* **1986**, *35*, 159. See also Refs. [1] and [40].
100. For a recent summary see Dunning, T. H., Jr.; Harding, L. B.; Wagner. A. F.; Schatz, G. C.; Bowman, J. M. *Science* **1988**, *453*.
101. Schatz, G. C. *J. Chem. Phys.* **1981**, *74*, 113.
102. (a) Truhlar, D. G.; Isaacson, A. D. *J. Chem. Phys.* **1982**, *77*, 3516. (b) Isaacson, A. D.; Truhlar, D. G. *J. Chem. Phys.* **1982**, *76*, 380.
103. (a) Walsh, S. P.; Dunning, T. H., Jr. *J. Chem. Phys.* **1980**, *72*, 1303. (b) Schatz, G. C.; Elgersma, H. *Chem. Phys. Lett.* **1980**, *73*, 21.
104. Rashed, O.; Brown, N. J. *J. Chem. Phys.* **1985**, *82*, 5506.
105. In a subsequent paper the reaction valley features for the OH + H_2 reaction obtained from a high quality *ab initio* surface will be discussed; Kraka, E.; Dunning, T. H., Jr. in preparation.
106. See, e.g., Dunning, T. H., Jr. *J. Phys. Chem.* **1984**, *88*, 2469 and references therein.
107. Harding, L. B.; Goddard, W. A. III. *Annu. Rev. Phys. Chem.* **1978**, *29*, 363.
108. Slater, J. C. *Quantum Theory of Atomic Structure*. New York: McGraw-Hill, 1960.
109. For experimental studies see on the OH + H_2 reaction, e.g., Smith, I. W. M; Zellner, R. *J. Chem. Soc. Faraday Trans. II* **1974**, *70*, 1045. Tully, F. P.; Ravishankara, A. R. *J. Phys. Chem.* **1980**, *84*, 3126. Frank, P.; Just, Th. *Ber. Bunsenges. Phys. Chem.* **1985**, *89*, 181. Madronich, S.; Felder, W. *J. Phys. Chem.* **1984**, *88*, 1857. Michael, J. V.; Sutherland, J. W. *J. Phys. Chem.* in press.
110. Zellner, R.; Steinert, W. *Chem. Phys. Lett.* **1981**, *81*, 568.
111. Glass, G. P.; Chaturvedi, B. K. *J. Chem. Phys.* **1981**, *75*, 2749.
112. Spencer, J. E.; Endo, H.; Glass, G. P. *Sixteenth Symposium (International) on Combustion*, p. 829. Pittsburgh, PA: Combustion Institute, 1977.

113. Light, G. C.; Matsumoto, J. H. *Chem. Phys. Lett.* **1978**, *58*, 578.
114. See, e.g., Ref. [99], and references therein.
115. For a recent review see also Kneba, M.; Wolfrum, J. *Annu. Rev. Phys. Chem.* **1980**, *31*, 47.
116. Elgersma, H.; Schatz, G. C. *Int. J. Quant. Chem. Symp.* **1981**, *15*, 611.
117. Schatz, G. C.; Colton, M. C.; Grant, J. L. *J. Phys. Chem.* **1984**, *88*, 2971.
118. Paldus, J. *J. Chem. Phys.* **1974**, *61*, 5321; Shavitt, I. *Int. J. Quantum Chem.* **1978**, *S12*, 5; Brooks, B. R.; Laidig, W. D.; Saxe, P.; Handy, N. C.; Schaefer; H. F. III *Phys. Scr.* **1980**, *21*, 312; Siegbahn, P. E. M. *J. Chem. Phys.* **1980**, *72*, 1647; Lischka, H.; Shepard, R.; Brown, F. B.; Shavitt, I. *Int. J. Quantum Chem.* **1981**, *S15*, 91; Saunders, V. R.; van Lenthe, J. H. *Mol. Phys.* **1983**, *48*, 923.
119. For a review of these technique see Bartlett, R. J. *Annu. Rev. Phys. Chem.* **1981**, *32*, 359 and Bartlett, R. J. *Comput. Phys. Rep.*, in press.